TECHNICAL UNIVERSITY OF CRETE

SCHOOL OF ELECTRICAL AND COMPUTER ENGINEERING

Hyperspectral dermoscope for the diagnostic and aesthetic analysis of the skin

Iliana Zacharopoulou

Thesis Committee:

Professor Costas Balas

Professor Michalis Zervakis

Associate Professor Vasilis Samoladas

June 2020

Table of Contents

List of Figures

List of Tables

Abstract

Hyperspectral Imaging is a powerful analytical tool that enables the acquisition of a series of images in narrow spectral bands. This technique makes it possible to combine both spatial and spectral information about the scene under investigation. Therefore, it is widely used for non-destructive and non-invasive analysis in various fields, ranging from food quality assessment to biomedical applications. The study of aging and the effects that causes on the human's skin texture has been for years investigated from both medical science and the cosmetic industry. For years, experts have relied on the evaluation of the human's skin texture with "naked eye" which has effects on the objective diagnosis and appropriate treatment. Until today, several imaging devices have been developed to contribute as additional tools for better and more objective diagnosis, but with several disadvantages that still affect it. The aim of this study is to develop an imaging system that will not only capture appearance of skin texture but also quantify it. Several approaches have been reported in the literature using image processing methods to analyze and quantify the texture of the skin, but restrict the analysis only in specific skin texture characteristics that are affected during the aging process. This study proposes a new method that is proving to be more effective and provides a quantitative assessment of skin texture characteristics, compared to the most widely used methods for this purpose, such as GLCM matrix, histogram and image processing in the frequency domain. Finally, using an innovative hyper-spectral dermoscope and a hyper-spectral imaging system, it is possible to collect images of the skin surface in narrow spectral bands extended beyond the visible spectrum perceived by the human eye. By using the appropriate image processing method and the appropriate spectral image band, more accurate and objective measurements can be extracted that will contribute to the objective diagnosis of specialists and the selection of more effective treatments.

Περίληψη

Η Υπερφασματική απεικόνιση είναι ένα πολύ ισχυρό αναλυτικό εργαλείο που επιτρέπει την απόκτηση μιας σειράς εικόνων σε στενές φασματικές ζώνες. Αυτή η τεχνική καθιστά δυνατή την απόσπαση τόσο της χωρικής όσο και της φασματικής πληροφορίας για τη σκηνή υπό διερεύνηση. Ως εκ τούτου, χρησιμοποιείται ευρέως για μη καταστροφική και μη επεμβατική ανάλυση σε διάφορους τομείς, που κυμαίνονται από την αξιολόγηση της ποιότητας των τροφίμων έως τις βιοϊατρικές εφαρμογές. Η μελέτη της γήρανσης και των επιπτώσεων που προκαλεί στο ανθρώπινο δέρμα έχει αποτελέσει εδώ και χρόνια αντικείμενο έρευνας τόσο στην ιατρική επιστήμη όσο και στη βιομηχανία θεραπευτικών καλλυντικών. Για χρόνια οι ειδικοί βασίζονταν στην αξιολόγηση της υφής του δέρματος με «γυμνό μάτι» με επιπτώσεις στην αντικειμενική διάγνωση και την αποτελεσματική θεραπεία. Μέχρι σήμερα αρκετές συσκευές απεικόνισης έχουν αναπτυχθεί με σκοπό να συμβάλλουν ως επιπλέον εργαλεία στην καλύτερη και πιο αντικειμενική διάγνωση έχοντας ωστόσο αρκετά μειονεκτήματα που εξακολουθούν να την επηρεάζουν. Στόχος αυτής της μελέτης είναι η ανάπτυξη ενός συστήματος απεικόνισης που όχι μόνο θα απεικονίζει την υφή του δέρματος αλλά και να την ποσοτικοποιεί. Στη βιβλιογραφία υπάρχουν διάφορες μέθοδοι επεξεργασίας εικόνας για την ανάλυση και την ποσοτικοποίηση της υφής του δέρματος με βάση τα χαρακτηριστικά της γήρανσης. Αυτή η μελέτη προτείνει μία νέα μέθοδο η οποία αποδεικνύεται ότι είναι πιο αποτελεσματική και παρέχει ποσοτική αξιολόγηση των χαρακτηριστικών της υφής, σε σύγκριση με τις πιο ευρέως χρησιμοποιούμενες μεθόδους για αυτό το σκοπό, όπως ο πίνακας συνεμφάνισης, το ιστόγραμμα και ο μετασχηματισμός της εικόνας στο πεδίο των συχνοτήτων. Τέλος, χρησιμοποιώντας ένα καινοτόμο υπερφασματικό δερματοσκόπιο είναι η δυνατή η συλλογή εικόνων της επιφάνειας του δέρματος σε στενές φασματικές ζώνες και εκτός του ορατού φάσματος που αντιλαμβάνεται το ανθρώπινο μάτι. Χρησιμοποιώντας την κατάλληλη μέθοδο επεξεργασίας εικόνας και την κατάλληλη φασματική ζώνη εικόνας μπορούν να εξαχθούν περισσότερο ακριβείς και αντικειμενικές μετρήσεις που θα συμβάλλουν στην αντικειμενική διάγνωση των ειδικών και στην επιλογή αποτελεσματικότερων θεραπειών.

Acknowledgements

First and foremost, I would like to express my gratitude to my professor and supervisor, Professor Constantinos Balas, for giving me the opportunity to deal with such an interesting topic. Not only did he help me completing my studies, but also motivated me to work more efficiently and professionally by conducting a lot of extra research, being familiar with experimental devices and gaining valuable knowledge.
Many thanks also goes to the whole team of the Optoelectronics & Imaging Diagnostics Lab", and especially,I am really grateful to Tsapras Athanasios (PhD Candidate), to Cristos Rossos (Phd Candidate) and to Anastasios Chatziioanou (Msc Researcher), for their invaluable help and cooperation, his time, advice and support through the research and implementation of this diploma thesis.
Finally, I want to thank my parents Georgios and Christina and my brother Ioannis for helping me selflessly to make my dream come true and supporting my decisions. Thank you

Part 1: Introduction

1.1 Introduction

For centuries, experts such as dermatologists, plastics surgeons or aesthetics have depended on their eyes and fingers to assess visible and tactile changes of the skin. Although "naked eye" assessment of the skin is important for skin examination and documenting changes before and after aesthetic procedures, it does not provide quantitative information.

Digital image analysis is a widely used method in beauty industry to study skin features and evaluate efficacy of skin care and cosmetic products. Nowadays, it becomes an extraordinarily powerful tool that may be used to not only capture appearance, but also measure it. Images define the nature and extent of the problem being treated, document before-and-after comparisons, and facilitate the monitoring of skin changes over time.
Skin imaging devices that visualize and display information about the skin conditions, have emerged as useful tools for skin analysis in aesthetic medicine. One obvious advantage of skin imaging devices is that they are non-invasive tools and allow enhanced clinical examination and improved methods of analyzing, grading and standardizing the results of therapeutic effects without interfering with the skin area.

Skin texture has become an important issue in recent research with applications in the cosmetic industry and medicine. Establishing a direct relationship between the human skin aging process and some characteristic properties of skin structural components is essential for quantitative assessment of the aging process. Many studies have been undertaken to date, most of them being focused on skin texture analysis.

The task assigned to this thesis is the possibility of using hyperspectral texture analysis to enrich the amount of information about skin aging. Spectral imaging combines spectroscopy and imaging. Each of these fields is well developed and is being used intensively in many fields including life sciences. The combination of these two is, however, not trivial, mainly because it requires creating a three-dimensional (3D) data set that contains many images of the same object, where each one of them is measured at a different wavelength.

First of all, we propose a new method for quantification of the skin texture and compare it with the most popular images processing methods in order to prove which is better for measuring and quantifying texture. Afterward, spectral images are acquired by the hyper-spectral imaging system and the Qcell Snapshot Hyperspectral Dermoscope, which are available at the Optoelectronics & Imaging Diagnostics Laboratory, and using the selected image processing method, we analyze skin surface texture with both of them.

1.2 Thesis Outline

Part 2 consists general information about the theoretical background about spectroscopy and spectral imaging.

In **Part 3** we analyze our proposal and the most commonly used image processing methods for quantification of the skin aging texture characteristics.

In **part 4** we show the results that extracted from each method and compare them with each other in order to choose the best image processing method for quantifying the skin texture.

Part 5 is the most important one, because it consists the hyperspectral analysis of skin aging characteristics using both a Snapshot Hyperspectral Dermoscope and a Hyperspectral Imaging system and discuss the results which obtained at each wavelength from these devices.

In **Part 6** we summarize the conclusions we were guided towards and the possible future research directions on the problem.

Part 2: Theoretical Background

2.1 Imaging

Imaging is the representation or reproduction of an object's form; especially a visual representation (i.e., the formation of an image). At this time, digital imaging is the most advanced and applicable method where data are recorded using a digital camera, such as a charged coupled device (CCD).

The amount of information that can be extracted from an image is determined by the quality of it, and the following list describes the most common parameters that characterize the acquired images.

- Spatial resolution determines the closest distinguishable features in the objects. It depends mainly on the wavelength (λ), the numerical aperture (NA) of the objective lens, the magnification, and the pixel size of the array-detector, usually a CCD camera. The latter two play an important role because they determine the sampling frequency which must be sufficiently high to achieve full resolution. Spatial resolution also depends on the signal quality.
- Lowest detectable signal depends on the **quantum efficiency** of the detector (the higher the better), the **noise level** of the system (the lower the better), the **NA** (numerical aperture) of the optics (the higher the better), and the **quality** of the optics.
- **Dynamic range** of the acquired data determines the number of different intensity levels that can be detected in an image. It depends on the maximal possible number of electrons at each pixel and on the lowest detectable signal (basically it is the ratio of these two values). If, however, the measured signal is low, so that the CCD well associated with a pixel is only partially filled, the dynamic range will be limited accordingly. As an example, if a CCD well if fulfilled to only 10% of its maximum capacity, the dynamic range will be reduced to 10% of its nominal value.
- **Field of view (FOV)** determines the maximal area that can be imaged.
- Other parameters include the exposure time range (usually determined by the detector) and the binning of the CCD pixels to gain sensitivity (by trading-off spatial resolution).

Category	*Property*	*Typical*
Imaging	Spatial resolution	250nm (in plane) at λ=500nm
	Field of view	~50 μm (high magnification)
	Dynamic range	8-16bits (256 – 65.536 intensity levels)
	Lowest detectable signal	Shot-noise limited
Spectroscopy	Spectral resolution	1-20nm (may depend on λ)
	Spectral range	400-900nm

Table 2. 1: Characteristics parameters of a spectral imaging system.

The use of imaging in dermatological diagnosis is currently a very rapidly growing branch of medicine and computer science. Computer-assisted medical diagnosis gives much wider possibilities than the methods of traditional evaluation performed by a medical diagnostician. The results obtained from computer analysis are automatic, re-producible, calibrated and independent of human factors related to both the patient and the medical diagnostician who performs the examination. The most common methods of imaging are ultraviolet, infrared and visible light. In this respect, the methods of assessment of various types of dermatological conditions, based on modern digital image processing and analysis methods of image are extremely popular.

As for imaging in visible light, a group of methods which enable morphometric measurements or profiled methods of image analysis and processing are used, for example, to determine the brightness of the RGB components in a segmented skin area. Hyperspectral imaging, which is also used in dermatology, offers much wider capabilities. Multispectral images are acquired using profiled multispectral cameras working in different spectra ranges. Additionally, depending on the frequency and spectrum range, various types of illuminators are used. Matching these two elements (camera and illuminator) is extremely important because of the need to obtain a flat spectrum of the illuminator (lamp) in the range covered by the camera.

2.2 Spectroscopy

Spectroscopy responds to the field of study including the interaction between matter and radiated energy. Historically, it is originated from the dispersion of visible light according to its wavelength. Later on, the concept was greatly expanded to comprise any interaction with radiative energy as a function of its wavelength (λ) or frequency (ν). As a result, the definition of spectroscopy was expanded to an alternative field, that one of frequency ν. A further extension added energy (E) as a variable, due to the equation $E = h \cdot \nu$. Spectroscopic data is often represented by a spectrum, meaning the plot of the response in proportion of wavelength or frequency [1] .

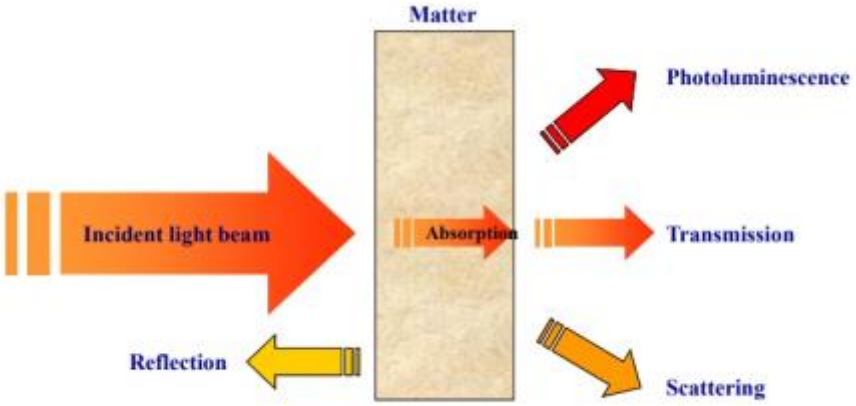

Figure 2. 1: How spectroscopy works

As it has been mentioned above, spectroscopy is strictly associated with the measurement of radiation intensity with reference to the wavelength or frequency. This sort of measurements can be conducted by experimental spectroscopic devices such as spectrometers, spectrophotometers, spectrographs or spectral analyzers

2.2.1 Electromagnetic Spectrum

The electromagnetic spectrum is the complete range of the wavelengths of electromagnetic radiation, beginning with the longest radio waves (including those in audio range) and extending through visible light (a very small part of the spectrum) all the way to the extremely short gamma rays that are a product of radioactive atoms. Visible light lies toward the shorter end, with wavelengths from 400 to 700 nanometers. Nearly all types of electromagnetic radiation can be used for spectroscopy, to study and characterize matter.

2.2.2.1 Range of the spectrum

Electromagnetic waves are typically described by any of the following three physical properties: the frequency f, wavelength λ, or photon energy E. Wavelength is inversely proportional to the wave frequency, so gamma rays have very short wavelengths that are fractions of the size of atoms, whereas wavelength on the opposite end of the spectrum can be of thousand kilometers. Photon energy is directly proportional to the wave frequency, so gamma ray photons have the highest energy (around a billion electron volts), while radio wave photons have very low energy (approximately a femtoelectronvolt). These relations are illustrated by the following equations:

$$f = \frac{c}{\lambda}, or\ f = \frac{E}{h}, or\ E = h * \frac{c}{\lambda}$$

The behavior of EM radiation depends on its wavelength. When EM radiation interacts with single atoms and molecules, its behavior also depends on the amount of energy per quantum

(photon) it carries.

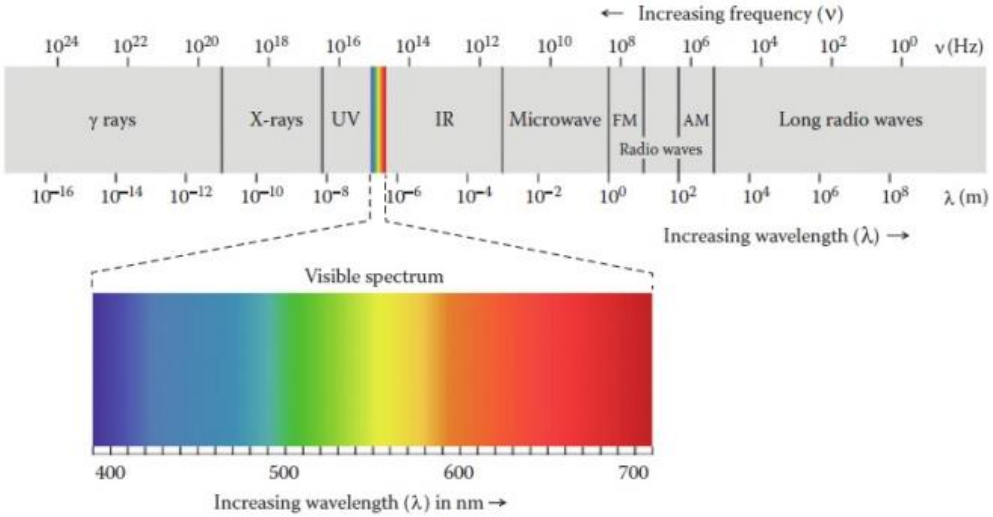

Figure 2. 2: Electromagnetic spectrum showing the visible light region

2.2.1.2 Visible spectrum

The **visible spectrum** is the part of the electromagnetic spectrum that is visible to the human eye. Electromagnetic radiation with a wavelength between 400 nm and 700 nm is detected by the human eye and perceived as visible light.

2.2.1.3 Reflectance spectrum of human skin

As we mentioned above, spectroscopy is the study of how substances absorb, transmit, or reflect light. Ultraviolet (UV),Visible(Vis) and Near infrared (NIR) spectroscopy is applied for optical absorbance and reflectance measurements in the wavelength range 200–1500 nm. Because a substance has its own unique reflectance characteristics, it can be distinguished by analyzing the light reflectance.

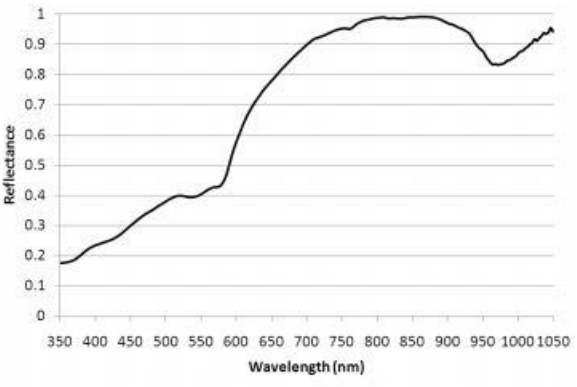

Figure 2. 3: Reflectance spectra of human skin

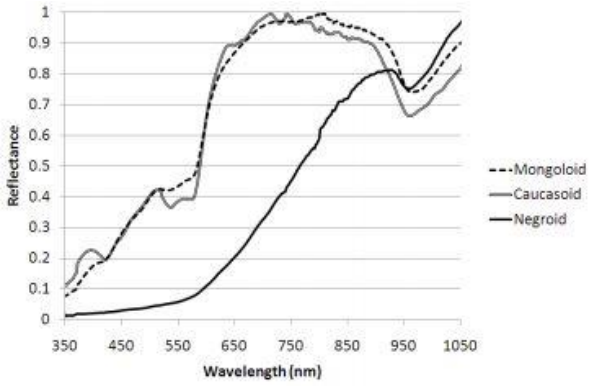

Figure 2. 4: Spectra of various human skin

Figure 2.3 shows only a reflectance spectrum of human skin. Skin has a lower reflectance at

shorter wavelengths (about 350nm) than at longer wavelengths (about 1050nm). In particular, skin has a unique property that it absorbs light around a wavelength of 970nm in the NIR region. Spectra of various human skin revealed that light was absorbed at a wavelength of 970nm, as shown in Figure 2.4.

2.3 Spectrometry

Spectrometry constitutes the technique that is being used so as to assess the concentration or amount of a specific chemical compound. It is a common practice to combine spectrometry along with spectroscopy, mentioned above, in physical and analytical chemistry for the identification of substances through the spectrum either emitted from or absorbed by them. In addition, they contribute to the field of astronomy and remote sensing as well. The majority of large telescopes is equipped with spectrometers, since the last ones have been instrumental to measurements, as far as chemical compositions and natural properties of astronomical objects are concerned.

2.4 Spectral Imaging (SI)

Spectral imaging is also known as imaging spectroscopy, which refers to the technology that integrates conventional imaging and spectroscopy methods to obtain both spatial and spectral information of an object. It was originally defined by Goetz in the 1980s and discussed for remote sensing of the Earth. Whereas the human eyes sees color of visible in mostly three (long wavelengths - perceived as red, medium wavelengths - perceived as green, and short wavelengths - perceived as blue), spectral imaging divides the spectrum into many more bands. This technique of dividing images into bands can be extended beyond the visible. Applications related to astronomy, solar physics, analysis of plasmas in nuclear fusion experiments, planetology, and Earth remote sensing are sparked by the benefits of spectral imaging.

Spectral imaging can be divided into Multi-spectral imaging, Hyper-spectral imaging (HSI), full spectral imaging, imaging spectroscopy or chemical imaging, according to its spectral resolution, number of bands, width, and contiguousness of bands. These terms are seldom applied to the use of only four or five bands that are all within the visible light range.

In spectral imaging, each pixel of the image collect spectral information, which is added as a third dimension to the two dimensional image, generating a three dimensional data cube, known as spectral cube. The spectral cube can be considered as a stack of images, each of them acquired at a different wavelength. Combined spatial and spectral information offers great potential for the non-destructive/invasive investigation of a variety of studied samples.

Spectroscopy finds application in analytical chemistry since a long time. Different spectroscopy types and modalities exist, depending on the optical property that it is intended to be measured, namely, absorption, spontaneous emission (fluorescence, phosphorescence), scattering (Rayleigh elastic, Raman inelastic) spectroscopy, etc. As the light travels into the sample, photons are experiencing absorption, which may result in fluorescence emission and multiple scattering due to the local variation of the index of

refraction. Spectrometers measure the intensity of the light emerging from the sample as a function of the wavelength. The collected light passes through a light-dispersing element (grating), which spatially splits the light wavelengths onto the surface of an optical sensor array, interfaced with a computer for recording and processing the spectrum. Sample illumination can be provided by either a broadband (e.g., white light) or a narrow-band light source. In the first case, the measured spectra provide information for the absorption and scattering characteristics of the tissue. In the second case, the measured spectra probe the fluorescence characteristics of the sample. Particularly, in steady-state fluorescence spectroscopy, a narrow-band light source is used for fluorescence excitation, such as lasers, LEDs, or filtered light sources, emitting typically in the blue-ultraviolet band. A sensitive optical sensor is used for collecting the emission spectra [2].

The collected emission spectra can provide diagnostic information for the composition of the sample. This makes spectroscopy an indispensable tool for non-destructive analysis and for the development of novel, non-invasive diagnostic approaches. Particularly, in biomedical sciences, the diagnostic potential of tissue spectroscopy is based on the assumption that the absorption, fluorescence, and scattering characteristics of the tissue change during the progress of the disease.

Over the last 20 years, spectroscopy has been extensively investigated as a tool for identifying various pathologic conditions on the basis of their spectral signatures. It had been demonstrated that spectroscopy can successfully probe intrinsic or extrinsic chromophores and fluorophores, the concentration of which changes during the development of the disease. In its conventional configuration, spectroscopy uses single-point probes that cannot easily sample large areas or small areas at high spatial resolution (SR). It is obvious that this configuration is clearly suboptimal when solid and highly heterogeneous materials, such as the biological tissues, are examined. In these cases, the collected spectrum is the result of the integration of the light emitted from a great number of area points. This has the effect of mixing together signals originating from both pathologic and healthy areas, which makes the spectral signature-based identification problematic. Looking at the same problem from another perspective, point spectroscopies are considered as inefficient in cases where the mapping of some characteristics, spectrally identifiable property, is of the utmost importance..

Spectroscopy probes optical signals with **high spectral resolution** but with **poor spatial resolution (SR)**. The vastly improved computational power together with the recent technological developments in tunable optical filter and imaging sensor technologies have become the catalysts for merging together imaging and spectroscopy. Both areas, imaging and spectroscopy, continue to be affected by technological innovations that enable faster acquisition of superior quality data. **SI has the unique feature of combining the advantages of both imaging and spectroscopy (high spatial and spectral resolution) in a single instrument**. In SI, light intensity is recorded as a function of both wavelength and location. In the image domain, the data set includes a full image at each individual wavelength. In the spectroscopy domain, a fully resolved spectrum at each individual pixel can be recorded. These devices can measure the spectral content of light energy at every point in an image. Multiple images of the same scene at different wavelengths are acquired for obtaining the spectra. As an example, an SI device integrating an imaging sensor with 1000×1000 pixels provides 1 million individual spectra. A spectrum containing 100 data points results from an equal number of spectral images. Assuming that the intensity in each pixel is sampled at 8

bits, then the size of the resulting spectral cube equals to 100 Mbytes. Due to the huge size of the collected data sets, SI data processing, analysis, and storage require fast computers and huge mass memory devices. Several mathematical approaches are used for spectral classification and image segmentation on the basis of the acquired spectral characteristics. The spectra are classified using spectral similarity measures, and the resulting different spectral classes are recognized as color-coded image clusters. SI can be easily adapted to a variety of OI instruments such as camera lenses, telescopes, microscopes, endoscopes, etc. For this reason, applications of SI span from earth observation including ground and atmosphere (remote sensing) to general medicine and molecular biology [3].

2.4.1 Spectral Reflectance

It has already been mentioned how materials print a spectral signature on the light they reflect. Different surface features reflect or absorb the sun's electromagnetic radiation in different ways. The reflectance properties of an object depend on the material and its physical and chemical state, the surface roughness as well as the geometric circumstances (e.g. incidence angle of the sunlight). The reflectance of a material also varies with the wavelength of the electromagnetic energy. Spectral reflectance represents the ratio between reflected and incident light, as a function of wavelength. This dependence is due to the fact that light is scattered or absorbed to different degrees at certain wavelengths, and it exists for almost every material.

There are several physical processes involved that determine the nature of the reflected light, and thus, the spectral signature of the material. In the first place, almost every object shows some degree of specular reflection, which means that some of the light rebounds directly on the surface of the material, as on a mirror. In this case, the spectrum of the reflected light remains the same as that of the incident light. There is no signature printed. In the second place, part of the light diffuses into the material where some is absorbed and some is randomly scattered, which is known as diffuse reflection. Finally, fluorescence, which is the emission of light by a substance that has absorbed light or other electromagnetic radiation, may also take place. In this case, a photon at shorter wavelength is absorbed and a photon at longer wavelength is emitted consequentially.

A white-colored material, for example, does not absorb any wavelength while a multi-colored material will absorb some wavelengths and diffusely reflect others. These reflected wavelengths are responsible for the color of the material. In a way, they shape the nature of the incident light to create what we perceive as color. This effect can be thought from the continuous spectrum point of view: it explains why matter prints a signature on the incident light depending on how different spectral components of light are absorbed or reflected.

2.4.2 The concept of Spectral cubes

The information that is collected by spectral imagers and then appropriately processed based on the kind of application running, is stored in 3D data structures for further analysis. This sort of data are known as Spectral Cubes**.** A spectral cube consists of the three dimensional projection of a great number of consecutive and registered sets of hyperspectral or multi-spectral images. For the accuracy, the first two dimensions respond to spatial dimensions, that is the pixel coordinates, and the third dimension refers to spectral dimension, which contains a specific wavelength of the electromagnetic spectrum. One of the important advantages of this technique is that it can acquire reflectance, absorption, or fluorescence spectrum for each pixel in the image, which can be used to detect several changes of objects that cannot be identified with traditional gray or color imaging methods. In the figure below shows the concept of a spectral cube.

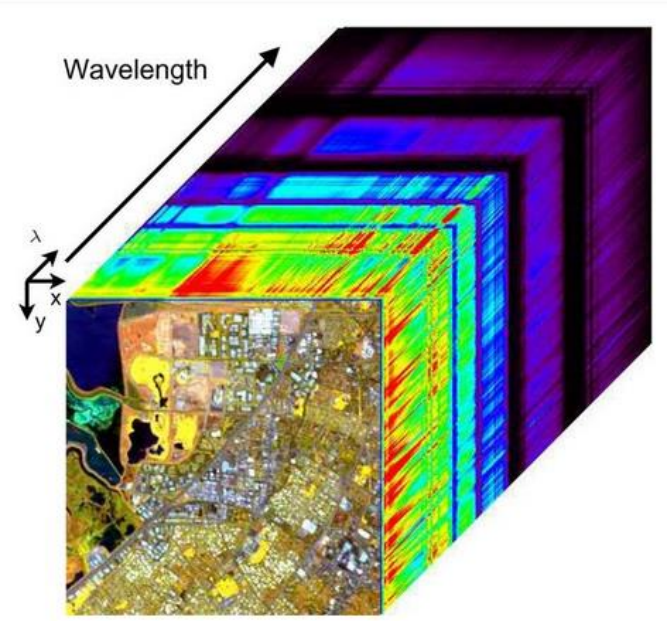

Figure 2. 5: Hyperspectral cubes

Simply put, an imaging spectrometer acquires the spectrum of each pixel in a two-dimensional spatial scene. As shown in Figure 2.6, the easiest way to think of such a scheme is a band sequential imaging, in which multiple images of the same scene at different wavelengths are acquired. A key point is that the spectra be sampled densely enough to reassemble a spectrum. There are many technological means of obtaining these data. The images are typically stacked in a computer, from the lowest wavelength to the highest, to create an image cube of the data set.

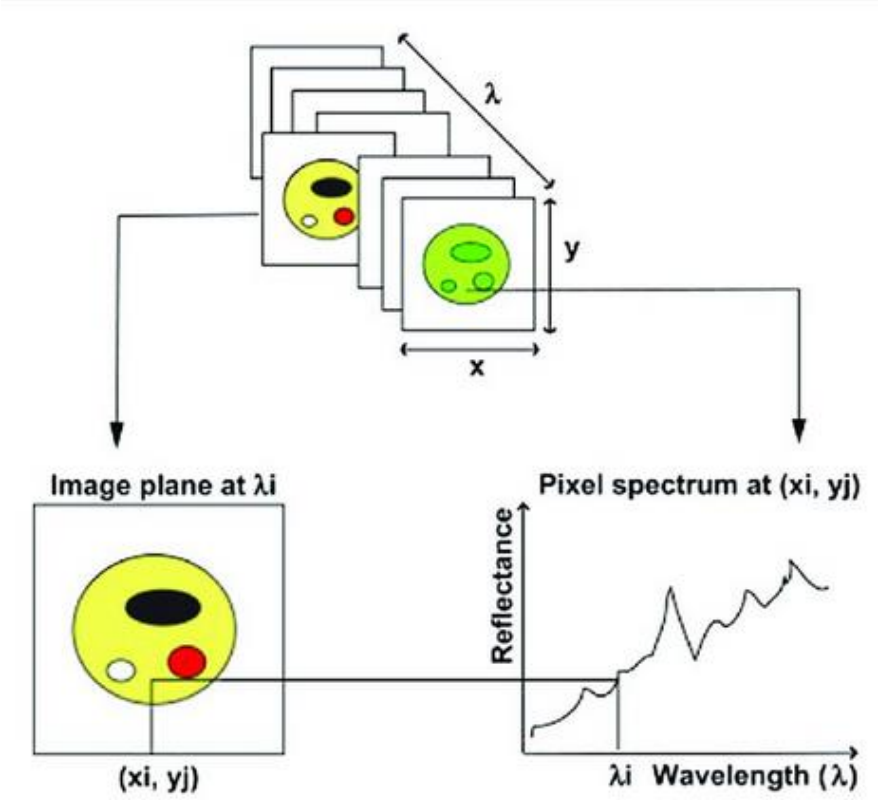

Figure 2. 6: Schematic representation of a hypercube showing the relationship between spatial and spectral dimensions.

The hyper-spectral cube consists of a series of contiguous sub-images one behind each other at different wavelengths. Each sub-image provides the spatial distribution of the spectral intensity at a certain wavelength. That means a hyper-spectral image described as $I(x, y, \lambda)$ can be viewed either as a separate spatial image $I(x, y)$ at each individual wavelength (λ), or as a spectrum $I(\lambda)$ at each individual pixel (x, y). From the first viewpoint, any spatial image within the spectral range of the system can be picked up from the hyper-spectral cube at a certain wavelength within the wavelength sensitivity. From the second viewpoint, the resulting spectrum of a certain position within the specimen can be considered as its own unique spectral fingerprint of this pixel to characterize the composition of that particular pixel.

2.4.2.1 Methods for hyperspectral Image acquisition

Hyperspectral images are three- dimensional [3-D] in nature. Generally there are four approaches that can be used for acquiring 3-D hyperspectral image cubes [hypercubes *(x, y, λ)*]. They are point scanning, line scanning, area scanning, and the single shot method, as illustrated in figure 2.8. In the **point-scanning** method (also known as the whiskbroom method), a single point (Fig. 2.8.a) is scanned along two spatial dimensions [x and y] by moving either the sample or the detector. A spectrophotometer equipped with a point detector is used to acquire a spectrum for each pixel in the scene. Hyperspectral image data are accumulated pixel by pixel in an exhaustive manner. Two-axis motorized positioning tables

are usually needed to finish the image acquisition. The **line-scanning** method (also known as the Pushbroom method) can be considered as an extension of the point-scanning method (Fig. 2.8.b). Instead of scanning one point each time, the method simultaneously acquires a slit of spatial information as well as spectral information corresponding to each spatial point in the slit. A special 2-D image [y, λ] with one spatial dimension [y] and one spectral dimension [λ] is taken at a time. A complete hypercube is obtained as the slit is scanned in the direction of motion [x]. Hyperspectral systems based on imaging spectrographs with either fixed or moving slits work in the line-scanning mode. Both point scanning and line scanning are spatial-scanning methods. The **area scanning** method (also known as band sequential method), on the other hand, is a spectral-scanning method (Fig. 2.8.c). This approach acquires a single band 2-D grayscale image (x, y) with full spatial information at once. A hypercube containing a stack of single band images is built up as the scanning is performed in the spectral domain through a number of wavelengths. No relative movement between the sample and the detector is required for this method. Imaging systems using filters (e.g., filter wheels containing fixed bandpass filters and electronically tunable filters) or Fourier transform imaging spectrometers belong to the area-scanning method. At last, the **single shot** method (Fig. 2.8.d) is intended to record both spatial and spectral information on an area detector with one exposure. No scanning in either spatial or spectral domains is needed for obtaining a 3-D image cube, making it attractive for applications requiring fast hyperspectral image acquisitions.

The 3-D hyperspectral image cubes acquired by point scanning, line-scanning, and are-scanning methods are generally stored in the formats of Band Interleaved by Pixel (BIP), Band Interleaved by Line (BIL), and Band Sequential (BSQ), respectively. Different formats have different advantages in terms of image processing operations and interactive analysis. The BIP and BSQ formats offer optimal performance for spectral and spatial accesses of the hyperspectral image data, respectively. The BIL format gives a compromise in performance between spatial and spectral analysis. The three data storage formats can be converted to each other. The single shot method usually utilizes a large area detector to capture the images. The spatial and spectral contents from each frame can be transformed in either format mentioned above using appropriate reconstruction algorithms.

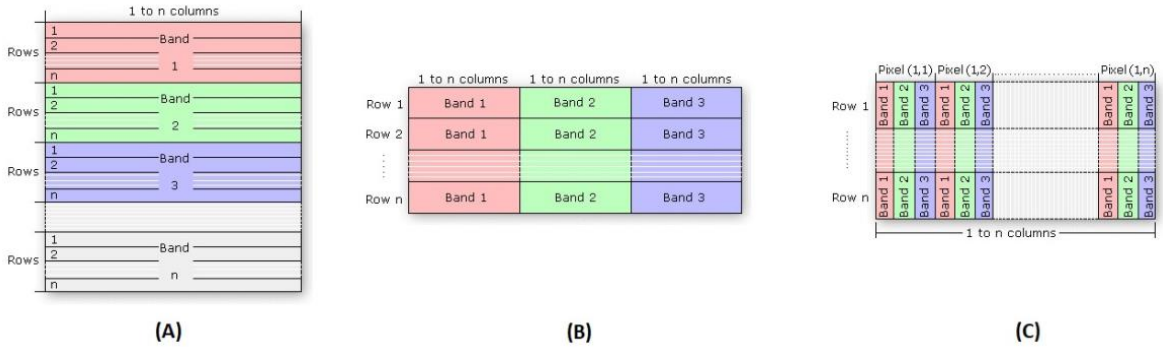

Figure 2. 7: The file layout of the: (A) BSQ, (B) BIL, and (C) BIP interleave.

2.4.2.2 Image sensing modes

A hyperspectral imaging system is generally carried out in **reflectance**, **transmittance** or **interactance** modes according to the specific light-output captured by hyperspectral imaging system. Position of light source and the optical detector (camera, spectrograph, and lens) are different for each acquisition mode. In reflectance mode, the detector captured the reflected light from the illuminated sample in a specific conformation to avoid specular reflection. External quality features are typically detected using reflectance mode, such as size, shape, color, surface texture and external defects. In transmittance mode, the detector is located in the opposite side of the light source (Fig. 2.8.f), and captures the transmitted light through the sample which carries more valuable internal information but is often very weak. Transmittance mode is usually used to determine internal component concentration and detect internal defects of relative transparent materials. However, transmittance mode has a low signal level from light attenuation and is affected by the thickness of sample. In interactance mode, both light source and the detector are located in the same side of sample and parallel to each other (Fig. 2.8.g).

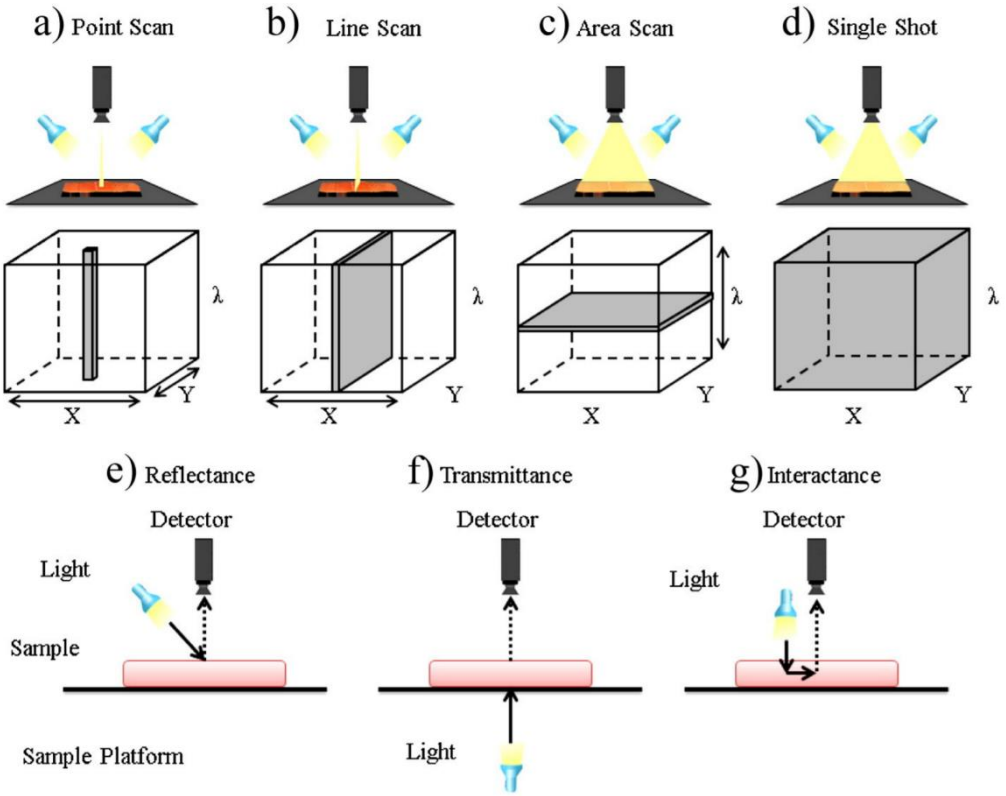

Figure 2. 8: Acquisition approaches of hyperspectral images and image sensing modes.

On the basis of such setup, the interactance mode can detect deeper information into the sample and has less surface effects compared to reflectance mode. Meanwhile, the interactance mode reduces the influence of thickness, which is a practical advantage over transmission. It should be noted that a special setup is required in the transmittance mode to seal light in order to prevent specular reflection directly entering the detector.

2.4.3 Color vs. Spectral Imaging

Photons encountering the pixels of an imaging sensor create electrons in pixel cells (photoelectric effect); thereby, the number of photons is proportional to the number of electrons. The photon's wavelength information, however, is not "transferred" to the electrons. Hence, unfiltered imaging chips are color blind. Color or SI devices employ optical filters placed in front of the imaging chip. Color imagers use either Si charge-coupled devices (CCD) or C-MOS sensors, which are sensitive in the visible and in the near-infrared (NIR) part of the spectrum (400-1000nm). A band-pass filter is used for rejecting the NIR band (700-1000nm). In 3-chip configurations, three photon channels are created with the aid of a trichroic prism assembly, which directs the appropriate wavelength ranges of light to their respective sensors. Camera electronics combine the red, green, and blue (R, G, B) imaging channels composing a high-quality color image, which is delivered to external devices through an analog or digital interface. An alternative, cheaper, and more popular color camera configuration employs a single chip, where the color filters are spread, similar to a mosaic, across all pixels of the sensor. Due to the fact that each pixel "sees" only one primary color, three pixels are required to record the color of the corresponding area of the object. This reduces significantly the standard range (SR) of the imager. This unwanted effect is partially compensated with a method called "spatial color interpolation" carried out by the camera electronics. The interpolation algorithm estimates the two missing primary color values for a certain pixel by analyzing the values of its adjacent pixels. In practice, even the most excellent color space interpolation methods cause a low-pass effect. Thus, single chip cameras yield images that are more blurred than those of 3-chip or of monochrome cameras. This is especially evident in cases of subtle, fiber-shaped image structures.

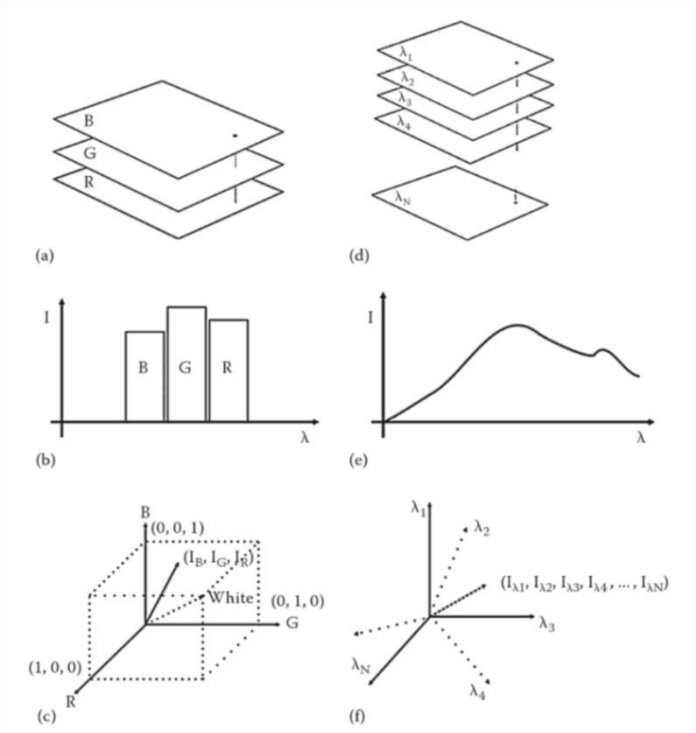

Figure 2. 9: Image data capturing and representation in color (a-c) and spectral (d-f) cameras

Color cameras emulate the human vision for color reproduction and are real-time devices since they record three spectral bands simultaneously at very high frame rates. Human vision-emulating color imaging devices usually describe color with three parameters (RGB values), which are easy to interpret since they model familiar color perception processes. They share, however, the limitations of human color vision. Color cameras and human color vision allocate the incoming light to three color coordinates, thus missing significant spectral information. Due to this fact, objects emitting or remitting light with completely different spectral components can have precisely the same RGB coordinates, a phenomenon known as **metamerism**. The direct impact of the metamerism is the inability of the color imaging systems to distinguish between materials having the same color appearance but different chemical composition. This sets serious limitations to their analytical power and consequently to their diagnostic capabilities [3].

Unlike images taken with standard color (RGB) cameras, SI information is not discernible to the human eye. In SI, a series of images is acquired at many wavelengths, producing a spectral cube. Each pixel in the spectral cube, therefore, represents the spectrum of the scene at that point. The nature of imagery data is typically multidimensional, spanning spatial and spectral dimensions (x, y, λ).

A color camera captures typically three images corresponding to the band-pass characteristics of the RGB primary color filters. Color image pixels miss significant spectral information as it is integrated into three, broad spectral bands. The color of a pixel can be represented as vector in a three-dimensional "color space" having the RGB values as coordinates. SI systems collect a stack of pictures, where each image is acquired at a narrow spectral band and all together compose the spectral cube. A complete spectrum can be calculated for every image pixel, which can be otherwise represented as a vector in a "multidimensional spectral space".

2.4.4 Multi-Spectral Imaging

Multi-Spectral Imaging (MI) is responsible for capturing image data at specific frequencies across the electromagnetic spectrum. The wavelengths may be separated by filters or by the use of instruments that are sensitive to particular wavelengths, including light from frequencies beyond the visible light range, such as infrared. MI images are the main type of images acquired by remote sensing (RS) radiometers. Dividing the spectrum into many bands, MI is the opposite of panchromatic, which records only the total intensity of radiation falling on each pixel. Multispectral imaging measures light in a small number (typically 3 to 15) of spectral bands. Spectral imaging with more numerous bands, finer spectral resolution or wider spectral coverage may be called **Hyper-Spectral** or **Ultra-Spectral.**

2.4.5 Hyper-Spectral Imaging

Hyperspectral imaging, known also as chemical or spectroscopic imaging, is an emerging technique that integrates conventional imaging and spectroscopy to simultaneously collect spatial and spectral information from an object. The term "hyperspectral imaging" was derived from works in remote sensing first mentioned by Goetz et al. in [4] to make a direct

identification of surface materials in the form of images. Although originally developed for remote sensing, hyperspectral imaging system is gradually found to have natural advantages over the traditional computer vision systems [5] in such diverse fields as agriculture [6–9]. With the development of optical sensing and imaging techniques, hyperspectral imaging has recently emerged as a scientific and efficient inspection and assessment tool for quality of fruits and vegetables. The goal of hyperspectral imaging is to obtain the spectrum for each pixel in the image of a scene, with the purpose of finding objects, identifying materials, or detecting processes [10]. To obtain high spectral resolution and narrow band image data, hyperspectral imaging is generally combined with spectroscopic technique, two-dimensional geometric space and one-dimensional spectral information detection.

2.4.6 Multi-Spectral vs. Hyper-Spectral Imaging

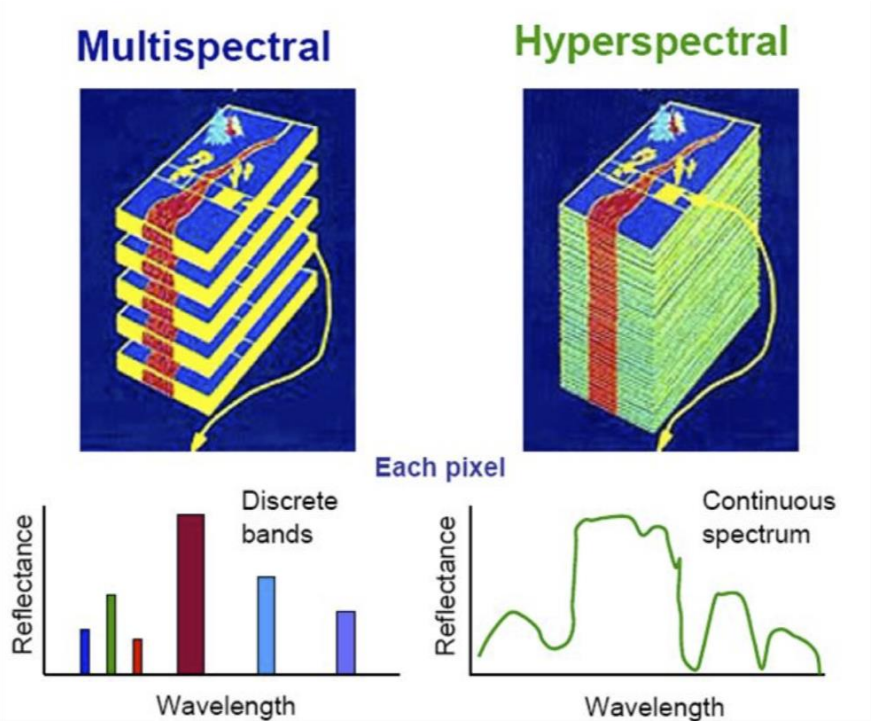

Figure 2. 10: Multi-Spectral vs. Hyper-Spectral Imaging

The main difference between multispectral and hyperspectral is the **number of bands** and **how narrow the bands are**. Multispectral imagery is produced by sensors that measure reflected energy within several specific sections (also called bands) of the electromagnetic spectrum. **Multis-spectral** also deals with several images at discrete and somewhat narrow bands. Being "discrete and somewhat narrow" is what distinguishes MI in the visible from color photography. MI images do not produce the "spectrum" of an object. **Hyperspectral sensors** measure energy in narrower and more numerous bands than multispectral sensors and produce the spectra of all pixels in the scene. The numerous narrow bands of hyperspectral sensors provide a continuous spectral measurement across the entire electromagnetic spectrum and therefore are more sensitive to subtle variations in reflected

energy. Images produced from hyperspectral sensors contain much more data than images from multispectral sensors. So, a sensor with only 20 bands can also be HI when it covers the range from 500 to 700 nm with 20 bands each 10 nm wide. Fig. 2.10 above helps us looking at the differences pinpointed above more closely.

2.6 Hyper-Spectral Analysis

Spectral analysis when combined with spatial data adds a significant amount of information that can be used to improve image exploitation and interpretation. To combine spectral information with spatial imagery, the sensor or camera has to be able to create images within the user defined narrow spectral bands rather than the wide-band imagery that the conventional cameras produce. Compared to conventional filter based imaging systems, spectral cameras provide higher spectral and spatial resolution, flexible wavelength selections in software, broader spectral coverage and shorter acquisition times.

2.7 Hyper-Spectral Cameras

Hyper-spectral analysis can be achieved by a hyper-spectral camera system that includes optics, an imaging spectrograph, a camera displaying the spectral information and a software package to display and calculate the results. Hyper-spectral cameras are used to acquire the hyper-spectral target image at tens or hundreds of wavelengths simultaneously. Such developed software creates new possibilities for imaging applications where spectroscopy methods can be totally attuned to standard and efficient image processing methods. The recorded full spectrum for each pixel of the image can be leveraged to a wide variety of purposes, such as classification, material detection, accurate color calculations or chemometrics over the full range [3].

2.7.1 SI Camera Hardware Configuration & Calibration

SI camera systems consist of a monochrome sensor, an electronically controlled spatial or spectral scanning mechanism, imaging optics, and a computer platform for storage, display analysis, and processing of imaging data. Control electronics synchronize the scanning and the data capturing processes, so that a set of spectral images are collected as members of the spectral cube [3].

The number of the spectral bands that an SI system is capable of acquiring determines the distinction between Multi-spectral imaging (MSI) and Hyper-spectral imaging (HSI). MSI devices typically acquire 5-20 spectral bands, while HIS systems acquire up to a few hundreds of spectral bands. Ultra-Spectral imaging (USI) devices are currently under development with capacity of acquiring thousands of very narrow spectral bands.

SI systems use monochrome sensors or sensor arrays, which can capture only two of the three spectral dimensions of the spectral cube at a time. To capture the third dimension, spatial or spectral scanning is required. Depending on the method employed for building the spectral

cube, SI devices are classified as follows:

1. **Whiskbroom** SI devices, where a linear sensor array is used to collect the spectrum (λ dimension) from a single point at a time; the other two spatial coordinates are collected with (x, y) spatial scanning.
2. **Pushbroom** SI devices in which a 2D sensor array is used, the one dimension of which captures the first spatial (x) coordinate and the other the spectral coordinate in each camera frame; the second spatial coordinate (y) is captured with line (slit) scanning.
3. **Staring** SI devices, where a 2D sensor array is coupled with an imaging monochromator, which is tuned to scan the spectral domain and in each scanning step, a full spectral image frame is recorded.

Whiskbroom and Pushbroom imagers utilizing spatial scanning for building the spectral cube do not provide live display of spectral images, since they are calculated from the spectra after the completion of the spatial scanning of the corresponding area. Staring imagers, on the other hand, are based on the tuning of the imaging wavelength and the spectra are calculated from the spectral cube composed by the spectral images that are captured in time sequence. Compared to the other approaches, staring imagers have the advantage of displaying live spectral images, which is essential for aiming and focusing.

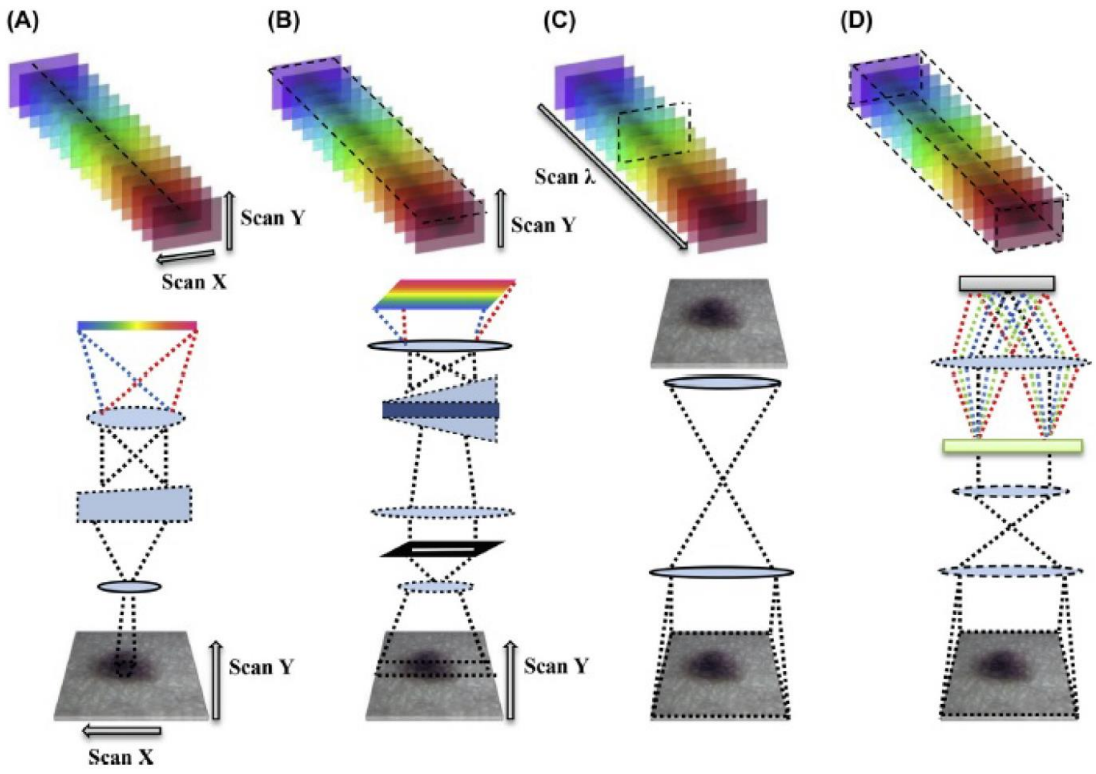

Figure 2. 11: Typical spectral imaging techniques. (A) Whiskbroom. (B) Pushbroom. (C) Staring. (D) Snapshot.

Selecting the SI camera optimal configuration and components requires a "system" approach. The intended application determines the SI system's spectral range and resolution. Si CCD detectors can be used to cover the spectral range ultraviolet (UV)-visible and NIR up to 1μm.

InGaAs detectors are suitable for the up to 1.7μm NIR range. For longer infrared wavelengths, HgCdTe or InSb cameras must be used. Ideally, the wavelength range of the monochromators should match at least a significant part of the spectral range within which the selected detector is sensitive. Narrowband imaging and monochromator optics reduce the overall light throughput of an SI system. Moreover, the light throughput of the monochromator depends on the wavelength. Furthermore, the quantum efficiency (QE) of the detector also changes with the wavelength.
Accurate calibrations for a hyperspectral imaging system are necessary to guarantee the stability and acceptability of the extracted hyperspectral image data and the consistent performance of the system. Even if the environment of data measurement is carefully controlled, inconsistent spectral profiles of reference spectra may be acquired by some systems. Therefore, it is necessary to eliminate this variability by using a standardized and objective calibration, and a validation protocol. The goals of calibration process are to standardize the spectral and spatial axes of the hyper-spectral image, validate the acceptability and reliability of the extracted spectral and spatial data, determine whether the hyper-spectral imaging system is in running condition, evaluate accuracy and reproducibility of the acquired data under different operating conditions, and diagnose instrumental errors if necessary.
SI system's calibration is very essential in order to achieve “device-independent" spectral measurements. Calibration can be performed with the aid of a reference sample displaying a known or a at spectrum over the entire operating wavelength range. A calibration curve or a lookup table can be obtained by comparing the known spectral characteristics of the calibration sample with that measured by the SI system spectra. Image brightness can be corrected on the basis of the calibration data, after spectral image acquisition. The calibration curve or the lookup table can also be integrated into the system's software for controlling the detector's exposure time during image acquisition, in all tuning steps of the filter. By changing the detector's exposure or gain settings, the wavelength dependence of the SI system's response is compensated and the spectral images that are acquired and captured are calibrated [1].

2.7.2. Scanning Spectral Imaging Systems Based on Electronically Tunable Filters

Spectral scanning SI systems can be categorized on the basis of the technological approaches employed for tuning the imaging wavelength. Two general classes of devices can be defined depending on whether their imaging monochromator contains or not moving parts. In the first case, mechanical parts, onto which filters or mirrors, etc. are mounted, are spatially translated for selecting the imaging wavelength. We can therefore name this category as **electromechanical tunable filters (EMTF)**. The second category refers to systems based on nonmoving optical modules whose spectral transmission can be electronically controlled through the application of voltage or acoustic signal, etc. For this reason, the members of this class of instruments are knows as **electronically tunable filters (ETF)**.

An alternative categorization could be done depending on whether the SI system provides or not live (real time) display of spectral images. A simple and rather trivial EMTF is a set of discrete band-pass filters, which are swapping in front of the sensor. The filters can be mounted on a rotating disk or on a translating stage. **Linearly variable filters (LVF)**, with transmission centre wavelength varying linearly along their surface, comprise an alternative

to discret filters option but they are more suitable as monochromators of the illuminating source. In all these cases, the motion of the filter arrangements is driven by a stepper motor, and in most cases, it is synchronized with the successive image capturing.

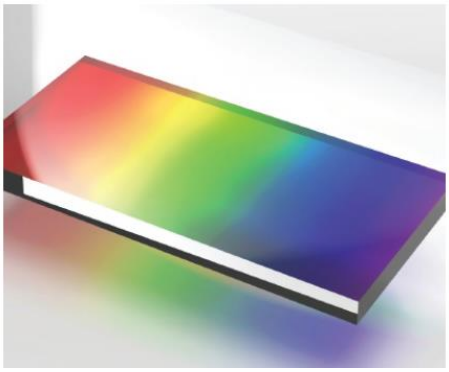

(a) Linearly Variable Band-pass Filter

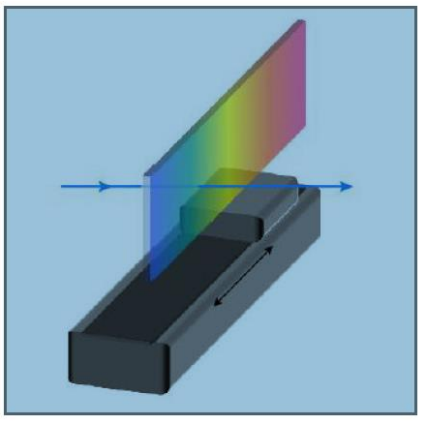

(b) Linearly variable filter; tuning is achieved by translating the filter along its length with a stage

Figure 2. 12: Linearly Variable Filters

A linear variable filter (LVF) is an optical interference filter whose spectral functionality varies along one direction of the filter, compared to a traditional optical filter whose spectral functionality is intended to be identical at any location of the filter. The term linear relates to the goal of making the wavelength variation a linear function of the position on the filter. The wavelength variation is achieved by an interference coating that is intentionally wedged in one direction, creating a linear shift of the center or edge wavelength along the same direction of the filter (fig. 2.13).

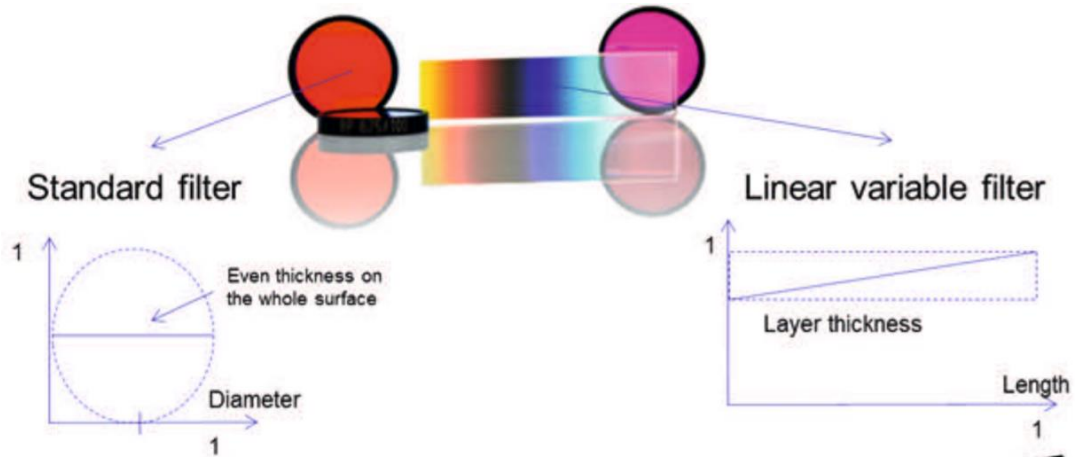

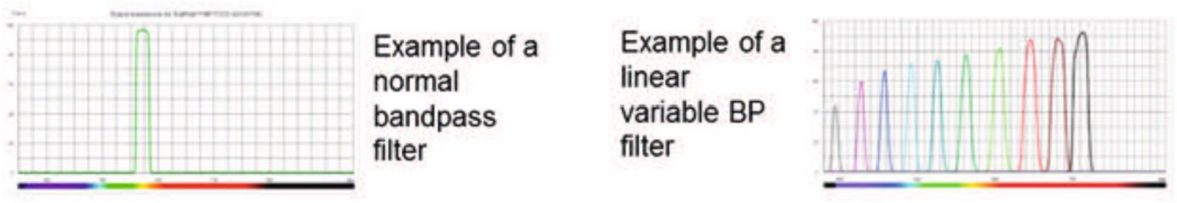

Figure 2. 13: Design Principle of standard and Linearly Variable Filter

2.8 Hyper-Spectral Imaging Applications

There are numerous applications emerging from the spectral analysis that is being provided by hyper-spectral imaging. For nearly a decade, this technology was primarily used for purposes like surveillance, reconnaissance, environmental and geological studies. However, the application of hyper-spectral imaging in the biomedical area has been negligible due to high-instrumentation costs and problems arising from the clinical use of hyper-spectral sensors. With recent achievements in sensor technology and increasing affordability of high performance spectral imagers, hyper-spectral imaging systems constitute one of the most important key areas in medical imaging. The early diagnosis of cancer, one of the most thorniest medical problems, is now possible, since the evolution of hyper-spectral sensors allows the scanning of a patient's body to identify precancerous lesions or to provide critical spectral data through endoscopic procedures. The extension and improvement of hyper-spectral imaging in biomedical and clinical diagnosis is within the grasp of researchers [11].
The advantages of this technology regarding diagnostic health care applications include a high-resolution imaging of tissues either at macroscopic or cellular levels and the capability to generate highly accurate spectral information related to the patient, tissue sample, or any other disease condition. In particular, the vast investment of hyper-spectral imaging in medicine lies on the generation of wavelength-specific criteria for disease conditions on spectral features. As a consequence, an ideal technology for high-throughput patient screening and non-invasive diagnosis is begotten.
Due to their unparalleled ability to reveal abnormal spectral signatures, hyper-spectral medical instruments hold great potential for non-invasive diagnosis of cancer, retinal abnormalities and assessment of wound conditions, for instance diabetes, etc. A portable hyper-spectral imager could also aid the analysis of human body fluids, such as blood, urine, saliva, semen and determine blood oxygenation levels of tissues, which could be of prime importance during surgeries. Yet importantly, it could perform diagnosis for dental diseases. It is a great advantage for a patient the fact that not only does an early diagnosis of an ailment take place, but an appropriate treatment may also be applied at the same time [3].
Hyper-spectral signatures when combined with targeting algorithms would in essence offer unique diagnostic information. There is an increasing level of interest on the part of health care providers to investigate possible ways of reducing health care costs by providing timely treatments for many types of disease conditions. Hyper-Spectral scanning imaging is expected to contribute a lot in this pursuit [2].

Part 3: Skin aging features analysis

3.1 Quantification of skin texture through digital image processing

Determination of skin surface texture is of particular importance in the field of dermatology as such measurements can be used for skin diagnostics and evaluation of therapeutic or cosmetic treatments. For centuries, experts such as dermatologists, plastics surgeons or aesthetics have depended on their eyes and fingers to assess visible and tactile changes of the skin. Although “naked eye” assessment of the skin is important for skin examination and documenting changes before and after aesthetic procedures, it does not provide quantitative information.

With the advances in technology the ability to document skin texture has become an adjunct methodology when evaluating a skin condition. In defining the texture of skin we are faced with the challenge of documenting a complex attribute, intimately connected to visual perception. Texture relates to the detailed geometry of the surface of skin as well as the mental factors that affect visual perception of texture. The task of measuring skin texture involves determination of parameters in different scales ranging from the organization of the corneocytes (at the cellular level, i.e. through electron microscopy or confocal microscopy) to the organization of skin microrelief lines and ⁄or surface glyphic structures (in the order of 10–100 lm, i.e. through video microscopy) and the measurement of larger features such as wrinkles and furrows (in the millimetric range, i.e. through close-up photography). In general, methods for in vivo skin texture measurements have to be noninvasive and nondestructive, hence optical methods are preferred.

Skin is the outermost part of the human body. It protects the body from infection, injury, and water loss, while helping regulate body temperature. Additionally, the skin maintains homeostasis and produces vitamin D. Skin performance is impaired with age and visual beauty is lost. This impairment and loss can proceed more quickly because of various factors, such as persistent sunlight exposure, smoking, and excessive drinking. Because of its visibility and role, considerable attention has been given to its condition, and substantial efforts have been taken to mitigate skin aging and damage progression.

To accurately access the skin condition, a method to objectively evaluate the skin is required. To date, this evaluation has been typically performed by dermatologists based on their personal experience and knowledge. Therefore, evaluation results can differ depending on the dermatologist. The degree of skin damage can be measured based on various features, such as texture pattern, skin elasticity, and moisture. Among these aspects, skin texture has the most visual effect and can be seen with the naked eye. A standard metric to evaluate the skin condition can be established using the diverse features of skin texture.

Therefore, by analyzing the texture of the skin by acquiring the texture image of the skin and exposing human skin to imaging devices, the health of the skin can be determined, but this is not enough. For a more accurate diagnosis or more effective treatment it is important to quantify the changes in the skin surface texture, according to the factors that affect it and that were mentioned.

In computer science, digital image processing concerns the transformation of an image to a digital format and its processing by digital computers. Image processing is a method to perform some operations on an image, in order to get an enhanced image or to extract some useful information from it. It is a type of signal processing in which input is an image and output may be image or characteristics/features associated with that image. Nowadays, image processing is among rapidly growing technologies. It forms core research area within engineering and computer science disciplines too. The three general phases that all types of data have to undergo while using digital technique are pre-processing, enhancement, and display, information extraction.

Several methods have been developed to measure skin texture aging damage. The texture discrimination can be obtained by choosing a set of attributes, the texture features, which account for the spatial organization of the image. Following are the most popular image processing algorithms and our proposal for analyzing and quantifying skin surface texture.

3.2 Digital image processing methods

3.2.1 Our Proposal Method

This method is based on the analysis of the spatial profile of an image in the spatial domain. It extracts information about the values of intensity, taken from regularly spaced points along a line segment or multi-line path in an image. Images are processed as follows:

- First the blue channel of the original image and its Spatial Profile are extracted. The blue channel is preferred, because it shows the greatest texture component and it used to quantify skin texture characteristics.
- Then, in the blue channel of the image is filtered with Gaussian blurring.

In image processing, a Gaussian blur (also known as Gaussian smoothing) is the result of blurring an image by a Gaussian function (named after mathematician and scientist Carl Friedrich Gauss). Gaussian blur is a low-pass filter. It is a widely used effect in graphics software, typically to reduce image and reduce detail. The formula of a Gaussian function in one dimension is:

$$G(x) = \frac{1}{\sqrt{2\pi\sigma^2}} e^{-\frac{x^2}{2\sigma^2}}$$

In two dimensions, it is the product of two such Gaussian functions, one in each dimension:

$$G(x, y) = \frac{1}{2\pi\sigma^2} e^{-\frac{x^2+y^2}{2\sigma^2}}$$

where x is the distance from the origin in the horizontal axis, y is the distance from the origin in the vertical axis, and σ is the standard deviation of the Gaussian distribution. When applied

in two dimensions, this formula produces a surface whose contours are concentric circles with a Gaussian distribution from the center point. Values from this distribution are used to build a convolution matrix which is applied to the original image. In theory, the Gaussian function at every point on the image will be non-zero, meaning that the entire image would need to be included in the calculations for each pixel. In practice, when computing a discrete approximation of the Gaussian function, pixels at a distance of more than 3σ have a small enough influence to be considered effectively zero. Thus contributions from pixels outside that range can be ignored.

From the intensity values of spatial profiles of the initial blue channel image and the smoothed one, the root mean square error value is calculated. The root-mean-square error (RMSE) or root-mean-square deviation (RMSD) is a frequently used measure of the differences between values (sample or population values) predicted by a model or an estimator and the values observed. The RMSE represents the square root of the second sample moment of the differences between predicted values and observed values or the quadratic mean of these differences. These deviations are called residuals when the calculations are performed over the data sample that was used for estimation and are called errors (or prediction errors) when computed out-of-sample.

RMSE is always non-negative, and a value of 0 (almost never achieved in practice) would indicate a perfect fit to the data. In general, a lower RMSD is better than a higher one. However, comparisons across different types of data would be invalid because the measure is dependent on the scale of the numbers used.

In this case, the predicted values are the values derived from the blurring image which representing the skin free of aging characteristics and the actual values are the values resulting from the analysis of the skin being studied. The root mean square error is defined as:

$$RMSE = \sqrt{\frac{\sum_{i=1}^{N} (Predicted_i - Actual_i)^2}{N}}$$

Therefore, this value is low when there are no significant fluctuations in the intensity of pixels of the image, so the Spatial Profile of the image will be smoother and its values will be close to the Spatial Profile values of the image after blurring.

On the contrary, when appears aging features to the skin (e.g. wrinkles, aging spots), there are significant fluctuations in the intensity, so the Spatial Profile of the initial blue image channel image will be rougher compared to the smoothed image and the difference between spatial profiles values is greater.

In this study, the spatial profiles for each image were analyzed in four different directions, starting from the analysis in the horizontal direction and rotating this line 45 degrees along the image and thus obtained four RMSE values in each direction. From these values the mean RMSE value is calculated. In this way, better accuracy in the analysis of skin texture is achieved and this value is more representative.

3.2.2 Grey Level Co-occurrence Matrix

GLCM is one of the effective methods for quantitative analysis of skin texture. This concept is proposed by Haralick in the 1970s, and it focuses on transforming the gray level information to texture information conveniently, which has been proven both in theory and experiments. It indicates the probability of gray-level *i* occurring in the neighborhood of gray-level *j* at distanced and direction y [12].

GLCM provides a supportive theory for the description of skin texture state. According to the principle of GLCM, if the image consists of pixel block, the diagonal element values of GLCM will be big. If the gray value of skin image pixel has a big change in some fields, the element values which keep away from the diagonal element will be big. As there is an internal mathematical relationship between GLCM and distribution of image texture, therefore GLCM has a good effect on skin texture analysis. It can evaluate skin texture, roughness and degree of consistency of skin condition. At present, the main characteristics parameters of GLCM for skin texture estimation, include angular second moment (ASM), contrast (Con), entropy (ENT), correlation (COR) and other indicators.

Texture c in total sets of value of imputing focuses on GLCM calculation. Take any point (x, y) in M*x*N image and another point (x+dx, y+dy) which deviates a s distance to form point pair and we assume the gray value of the point pair is (g1,g2). To begin with, the point (x, y) is moved on the whole image and several different values of (g1, g2) are acquired. Then the series of image gray values is supposed as k, and there will be k^2 sets of value of (g1, g2) in total. For the whole picture the frequency of every (g1, g2) is counted and arranged them in a matrix. Moreover, according to the total number of appearing (g1, g2), the matrix members need to be normalized transformed into the probability P(g1, g2). This matrix is called, the GLCM matrix. As can be seen from it, GLCM is a function of distance and direction whose order is determined by gray values of the image and it is a symmetrical matrix. When (dx, dy) has different values it can be obtained joint probability matrix in different situations. The value of (dx, dy) should be chosen from distribution of texture. Small divided difference need to be acquired for the thinner texture, for example, (1, 0), (1, 1), (1, 1), (-1, -1). At the same time, calculating the four individual orientations (0, 45°,90°,135°) reflects the statistics features of skin texture comprehensively, according to the concept of pixel neighborhood.

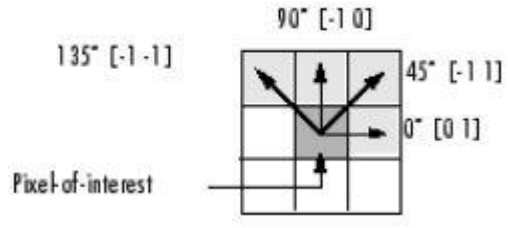

Figure 3. 1: Distance between the pixel of interest and its neighbor

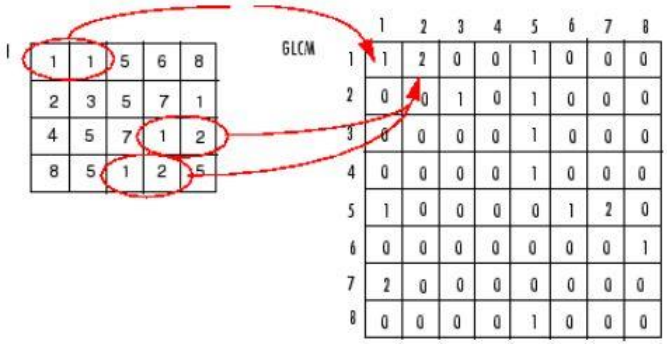

Figure 3. 2: Shows how graycomatrix calculates several values in the GLCM of the 4-by-5 image I.

The main features extracted from this table are the following:

- **Angular Second Moment (ASM):** also called energy and is a measure of textural uniformity of an image (the thickness measurement of the image texture). Energy reaches its highest value when gray level distribution has either a constant or a periodic form. A homogenous image contains very few dominant gray tone transitions, and therefore the P matrix for this image will have fewer entries of larger magnitude resulting in large value for energy feature. In contrast, if all element values of P matrix are equal, the ASM is small. Therefore, the ASM value is maximum when the skin texture situation is the best. The definition of Angular Second Moment is:

$$Asm = \sum_{g_1}\sum_{g_2}[p(g_1,g_2)]^2$$

- **Entropy (ENT):** measures the disorder of an image and it achieves its largest value when all elements in P matrix are equal. When the image is not texturally uniform many GLCM elements have very small values, which implies that entropy is very large. Therefore, entropy is inversely proportional to GLCM energy, so its value is minimum when the skin texture situation is the best. Entropy is calculated from the following formula:

$$ent = -\sum_{g_1}\sum_{g_2} p(g_1,g_2)\lg p(g_1,g_2)$$

- **Contrast (CON):** Contrast is a difference moment of the P and it measures the amount of local variations in an image and is defined as:

$$con = \sum_{k} k^2 \left[\sum_{g_1}\sum_{g_2} p(g_1,g_2)\right]$$

Where $k=g_1-g_2$.

- **Correlation (COR):** Correlation is used to measure the similar extent of GLCM elements in a certain direction. Its definition of COR is:

$$cor = \frac{\sum_{g_1}\sum_{g_2} g_1 g_2 p(g_1,g_2) - \mu_x\mu_y}{\sigma_x\sigma_y}$$

3.2.3 Fast Fourier Transform (FFT) – Butterfly pattern

In digital image processing, the most ordinary way to represent an image is in the spatial domain by column (χ), row(y) and value (z). But sometimes image processing routines may be slow or inefficient in the spatial domain, requiring a transformation to a different domain that offers compression benefits. A usual transformation is from the spatial domain to the frequency (or Fourier) domain. The frequency domain is the basis for many image filters which used to remove noise, sharpen an image, analyze repeating patterns, or extract features and pixel location is represented by its x- and y-frequencies as its value is represented by amplitude.

Digital images, unlike light wave and sound wave in real life, are discrete because pixels are not continuous. That means it should be implemented Discrete Fourier Transformation (DFT) instead of Fourier Transformation. However, DFT process is often too slow to be practical. The Fast Fourier Transform is the most used method to transform an image from spatial domain into the frequency domain and decomposes an image into its real and imaginary components. The number of frequencies is equal to the number of pixels in the spatial domain of an image. Low frequencies represent gradual variations and they contain the most information because they determine the overall shape or pattern in the image. Also they are often shown by a large peak in the center of the data. High frequencies correspond to abrupt variations in the image and they provide more detail, but they contain more noise.

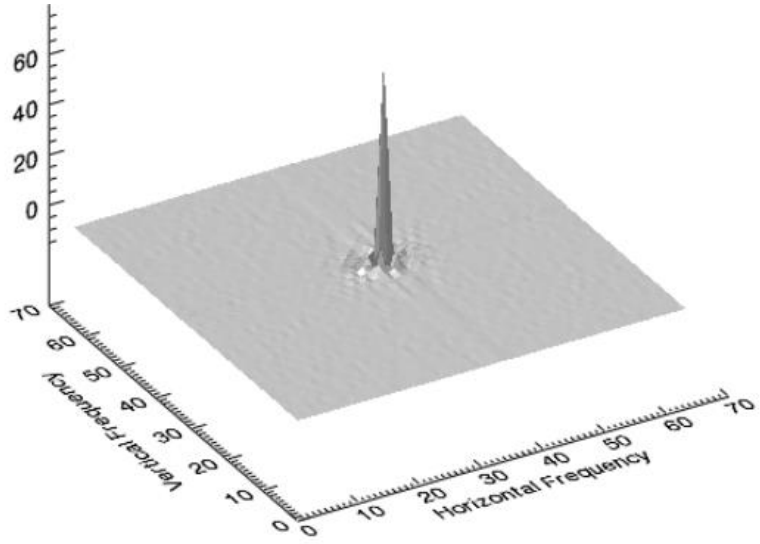

Figure 3. 3: The lowest frequencies are shown by a large peak in the center of the data.

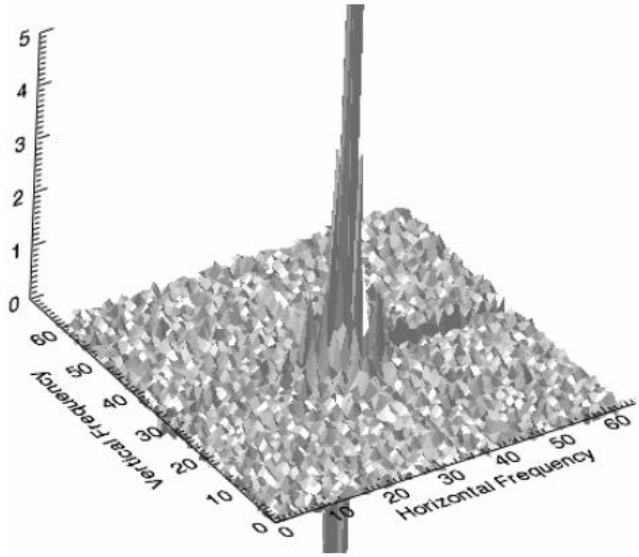

Figure 3. 4: Low frequencies in the center and high frequencies around which reveals that the image has some background noise.

The Fourier transform of a MxN image described by Jean-Baptiste-Joseph Fourier in 1807 and given by following equation:

$$F(u,v) = \int_{\infty}^{\infty} \int_{\infty}^{\infty} f(x,y) e^{-j2\pi(ux+vy)} \, dxdy$$

Where ƒ(x,y) is an image function and this expression must be computed for values of u = 0, 1, 2, ..., M− 1 and also for v = 0, 1, 2, ...N – 1. Similarly, the same function can be represented in the Fourier domain without loss of information due to transforming an image between spatial and frequency domain using inverse Fourier transform:

$$f(x,y) = \int_{\infty}^{\infty} \int_{\infty}^{\infty} F(u,v) e^{j2\pi(ux+vy)} \, dudv$$

The image processing algorithm using FFT transform is as follows:

Step 1: Computing Fast Fourier Transform of a gray scale image.

The result from FFT process is a complex number array which is very difficult to visualize directly. Therefore, we have to transform it into 2-dimension space. There are two ways which can visualize this FFT result, Spectrum and phase angle. Here is an example:

In the spectrum image there are some symmetric patterns on the four corners. The white area show the high power of frequency. The corners in the spectrum image represent low frequencies. Therefore, combining two points above, the white area on the corner indicates that there is high energy in low/zero frequencies which is a very normal situation for most images.

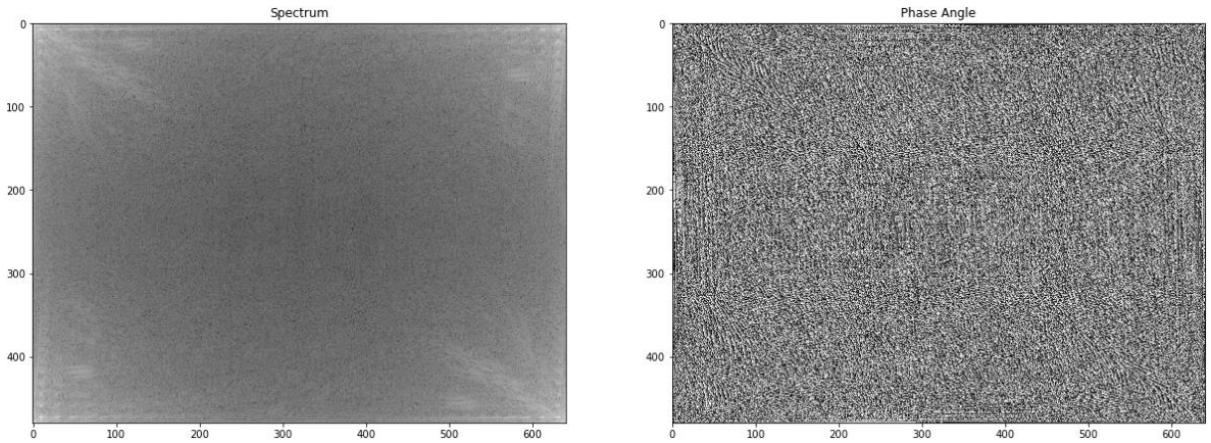

Figure 3. 5: (From left to right) Spectrum and Phase Angle

On the other side, it is hard to identify any noticeable patterns from phase angle image. This did not indicate that the phase angle of FFT is useless because, the phase preserves the shape characteristics which is an indispensable information for an image.

Step 2: Shift the zero-frequency component to the center of the spectrum.

2-D FFT has translation and rotation properties, so it can shift frequency without losing any

piece of information. When the zero-frequency component shifted to the center of the spectrum, makes the spectrum image more visible for human. Moreover, this translation helps to implement high/low-pass filter easily.

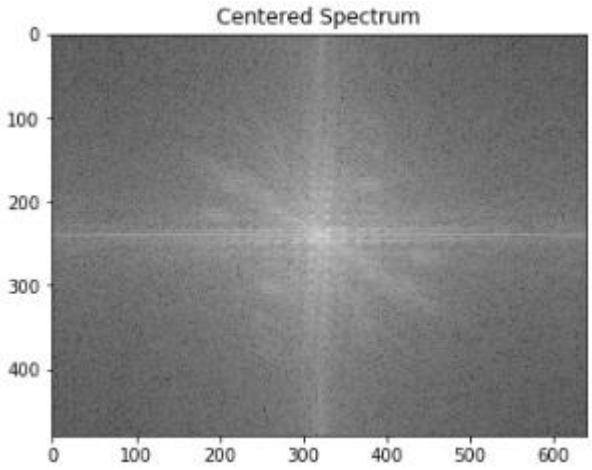

Figure 3. 6: Centered Spectrum after shifting the zero-frequency component

Step 3: Inverse of Step 2. Shifting the zero-frequency component back to original location.

Step 4: Inverse of Step 1. Computing of the 2-dimensional inverse Fast Fourier Transform.

The processes of step 3 and step 4 are converting the information from spectrum back to gray scale image. It could be done by applying inverse shifting and inverse FFT function.

In this approach the analysis of skin texture based on the imaging of micro-relief of the skin surface texture. An important feature of micro-relief is its pattern that is, the two-dimensional relationship between primary and secondary lines (skin texture) and its grade of irregularity. Using fast Fourier transform (FFT), it was possible to convert the space field into the frequency field and to obtain important information on this feature of the skin. The Fourier Transform is used in this case because it needed access in the geometric characteristics of skin surface micro-relief. Because the image in the Fourier domain is decomposed into its sinusoidal components, it is easy to examine or process certain frequencies of the image, thus influencing the geometric structure in the spatial domain.

In the frequency field, skin network line set is allowed to be displayed as a series of light points, more or less assembled depending on the regularity of the pattern. According to this method, the micro-relief of a young and an older skin shows different drawings. In the young skin pattern, primary and secondary lines are clearly visible and nearly of the same depth. Their cross points form a ‘‘star’’ pattern (like apexes of triangles converging at the same point). In aged skin, primary lines are more evident than secondary ones and the pattern is flattened and almost directional, not being able to form repeated regular geometrical figures.

So, in that case image function $f(x,y)$ is a skin micro-relief image in black and white representation. In the frequency domain, the disposition of pixels varies from a ‘‘butterfly’’ pattern at younger ages, representing a very regular texture, to a directional one as the skin ages (see Fig 3.7). Therefore, the image processing includes only step 1 and step 2, because we need the image spectrum to represent these skin micro-relief patterns in the frequency domain.

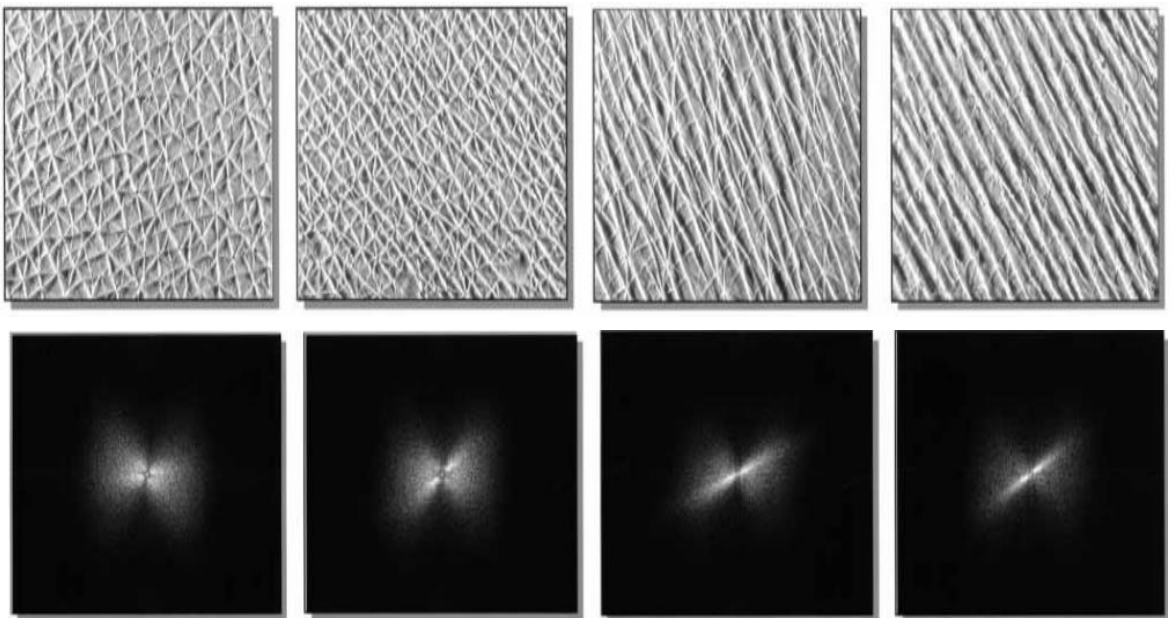

Figure 3. 7: Various patterns of skin texture on the lateral aspect of the thighs and corresponding FFT

By means of irregularity skin index, it was possible to quantify skin texture variations that correlated with the intrinsic ageing process. To quantify the irregularity grade of each texture, two curves from the density of pixels are calculated. Irregularity skin index (ISI) of the u and v axis represent the integrals of area delimited by the two curves derived from the density of pixels in the u and v axis. According to this, as age increases, the irregularity skin indexes increases too [13].

3.2.4 Fast Fourier Transform (FFT) – Butterworth Filtering

This method is also based on image analysis and processing in the frequency domain for the evaluation of skin surface roughness. Compared to the previous method, the Fourier transform is used to enhance the image by filtering it in the frequency domain, in order to highlight specific features that represent roughness of the skin. Image enhancement, can be done in the spatial domain using both linear and non-linear filters or in the frequency domain using linear filters. The new image *g*(x,y) after filtering is the result of the convolution of the original image *f*(x,y) with a mask *h*(x,y) of a linear filter:

$$g(x,y) = f(x,y) * h(x,y)$$

The corresponding procedure in the frequency domain is based on that the convolution in the spatial domain is equivalent to the product of the spectrums in the frequency domain:

$$G(u,v) = F(u,v)H(u,v)$$

Frequency Domain Filters are used for smoothing and sharpening of image by removal of high or low frequency components. Sometimes it is possible of removal of very high and very low frequency.

Frequency domain filters are different from spatial domain filters as it basically focuses on the frequency of the images. It is basically done for two basic operation i.e., Smoothing and Sharpening.

These are of 3 types:

1. **Low pass filters:** Low pass filter removes the high frequency components that means it keeps low frequency components. It is used to smoothen the image by attenuating high frequency components and preserving low frequency components.
2. **High pass filters:** High pass filter removes the low frequency components that means it keeps high frequency components that represents the edges of an image and it is used for sharpening the image.
3. **Band pass filters:** Band pass filter removes the very low frequency and very high frequency components that means it keeps the moderate range band of frequencies. Band pass filtering is used to enhance edges while reducing the noise at the same time.

According to this method, the image function *f*(x,y) is the blue channel of a given image (B-delta image), which is converted to the frequency field by the Fourier transform. Then, the image in the frequency domain is filtered with Butterworth low-pass digital filter to decrease the contribution from the skin area curvature. Moreover, in the same image, a high-pass Butterworth filter is applied to sharpen the image and show how rough the surface of the skin is. The transfer function of a Butterworth low-pass filter of order n with cutoff frequency at distance D_0 from the origin is defined as:

$$H(u,v) = \frac{1}{1 + \left[\frac{D(u,v)}{D0}\right]^{2n}}$$

The Butterworth high pass filter given as:

$$H(u,v) = \frac{1}{1 + \left[\frac{D0}{D(u,v)}\right]^{2n}}$$

The basic steps to filter an image in the frequency domain using Fast Fourier Transform are the following:

1. First we calculate the Fourier Transform of an image, *F(u,v).*
2. Subsequently, we multiply the transformation *F(u,v)* by the filter transfer function *H(u,v).*
3. We calculate the inverse Fourier Transform of the result of step 2.
4. We use only the real part of the result of step 3.

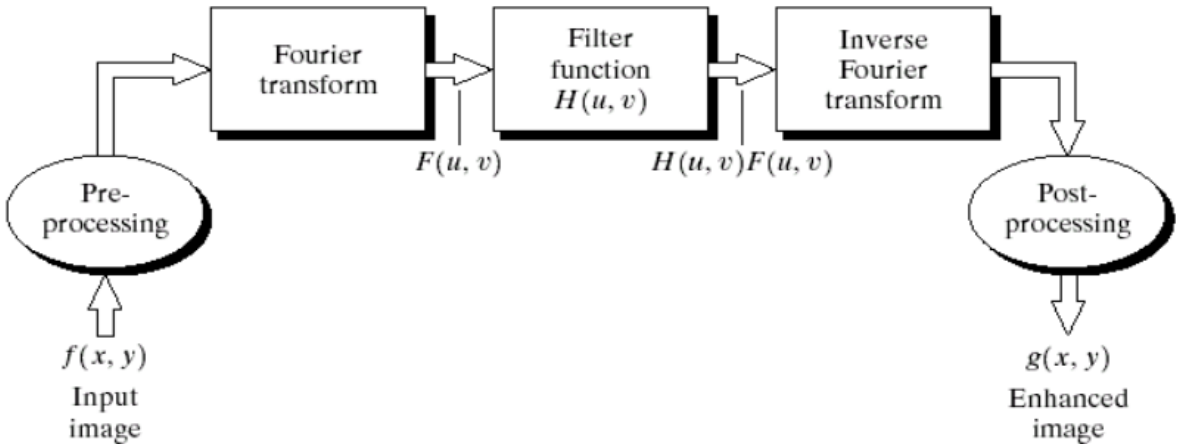

Figure 3. 8: Frequency domain filtering operation

Skin texture can be determined by measuring the width of the intensity distribution (histogram) of the B-delta image, which is proportional to the roughness of the sample. A rougher sample, e.g. the skin of an older person, will have a wider intensity distribution due to the larger dimension and the heterogeneity of the topographical landmarks (such as wrinkles, fine lines etc.). Also, the skin texture image of an older person will be more sharpened after filtering with high pass Butterworth filter than a younger person. In case of image filtering with a low-pass Butterworth filter, the resulting smoothed image of a young person will be appear more uniform, in contrast with the smoothed image of an older person (fig. 15,16) [14].

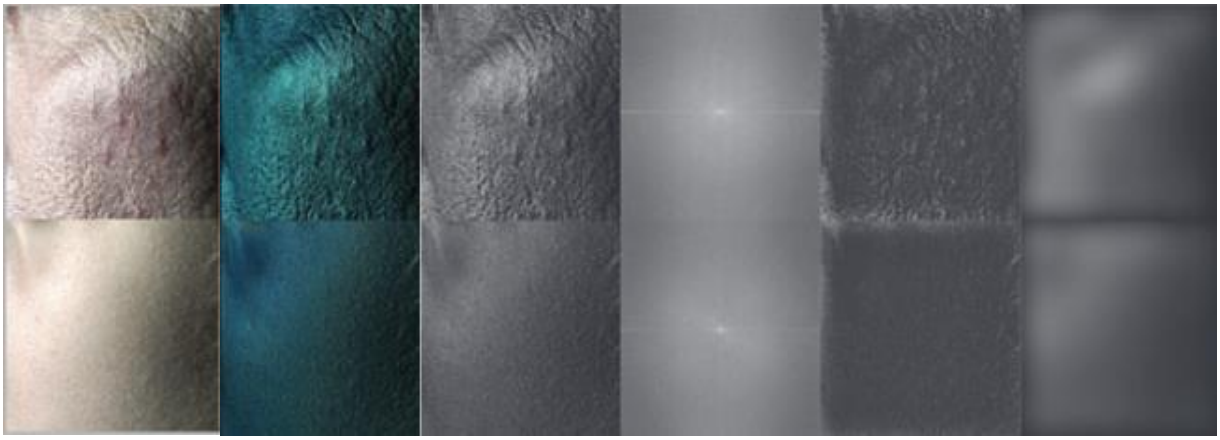

Figure 3. 9: Image processing steps. From left to right the images are: copolarized perpendicular orientation;); blue channel of the delta image (B-delta image); Fast Fourier Transform of the B-delta image; the high-frequency component of the B-delta image; and the low-frequency component of the B-delta image. The top row shows the images for the old subject and the bottom row for the young subject.

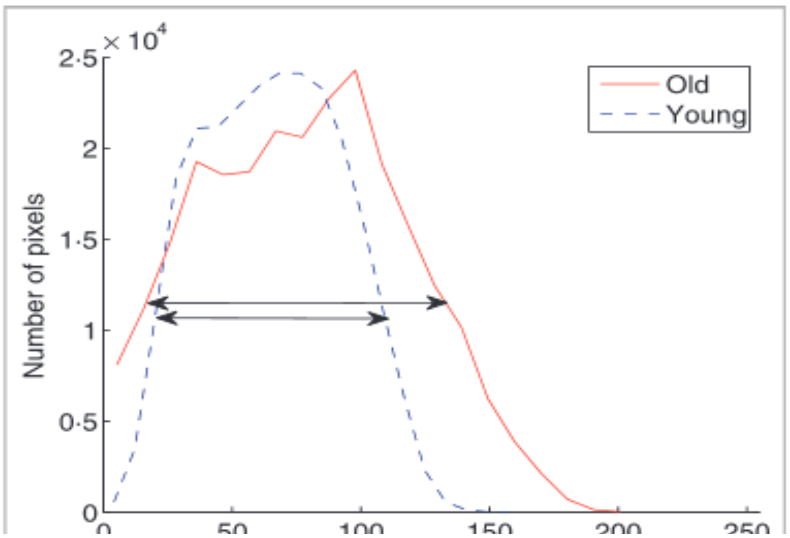

Figure 3. 10: The pixel intensity distribution of the B-delta images for the old and young subjects of Figure 3. The width of the distribution for the older subject (rougher skin) is larger than that of the young subject as pointed by the arrows.

Part 4: Measurements and Results

4.1 Skin Surface Texture Analysis

In this section we compare the results obtained by analyzing images of skin surface samples, with the most popular image processing techniques for measuring and analyzing skin surface texture, that have been collected and described previously (see Part 3). In a first stage, the images of skin surface texture that we have collected from the internet were used in each method, in order to select which one is better and more accurate to analyze and quantify skin surface texture. These images represent different skin surface textures and different skin color types as shown below.

(1)

(2)

(3)

(4)

(5)

(6)

(7)

(8)

(9)

(10)

Figure 4. 1: Skin surface texture samples collected from the Internet.

Observing the above images with «naked eye», it seems that images 1,2 and 3 have the smoothest skin surfaces textures compared to the others, while the most intense skin lesions are shown in Figures 8,9 and 10. Figures 4-7 can be described as an average skin condition compared to the rest (neither smooth nor intense lesion of the skin surface texture).

4.1.1 Results from our Proposal Method

The following graphs show the intensity profiles of all the above images and the table shows the corresponding RMSE values derived from the values of the intensity profiles of the blue channel of images. Assuming that all images have the same dimensions NxM, then the line from which the intensity profile of each image is calculated, has the point (N/2, 0) as starting point and the point (N/2, M-1) as the end point. The size of the Gaussian filter which is used to blur the image is hsize=15 with standard deviation σ=8 on 183x279 image size.

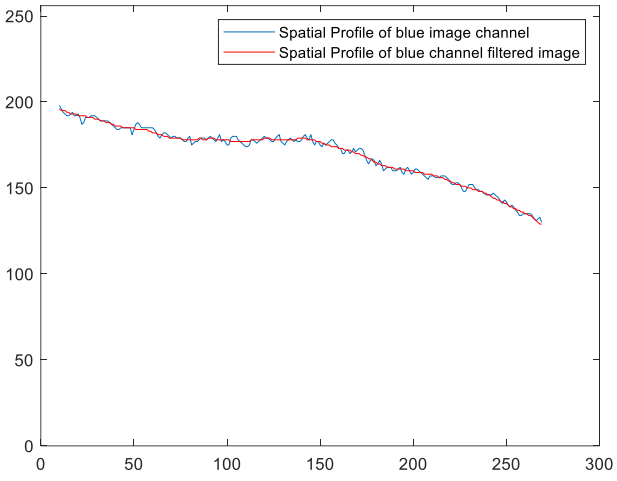

(1) RMSE=1.64

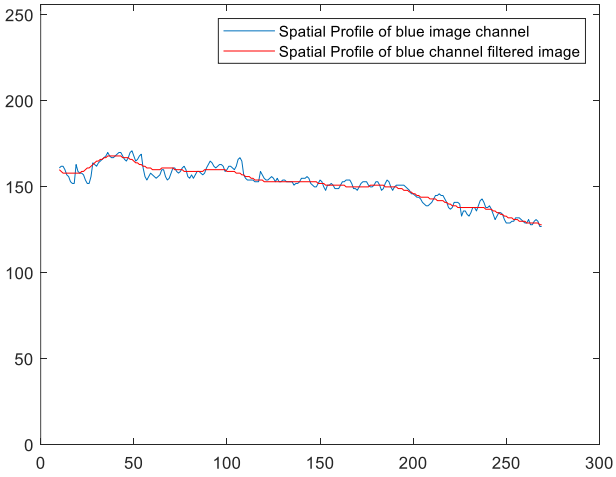

(2) RMSE=2.79

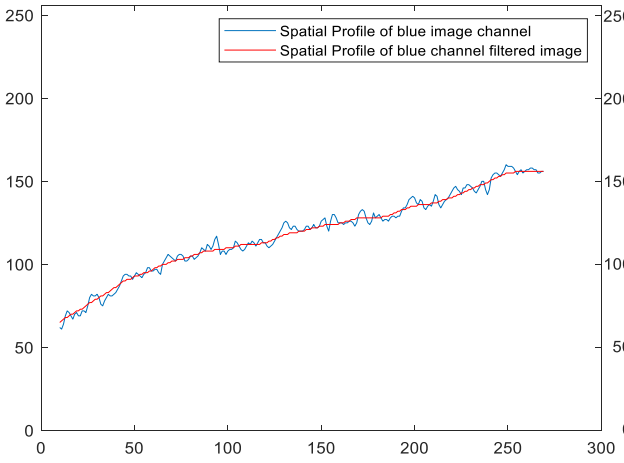

(3) RMSE=2.83

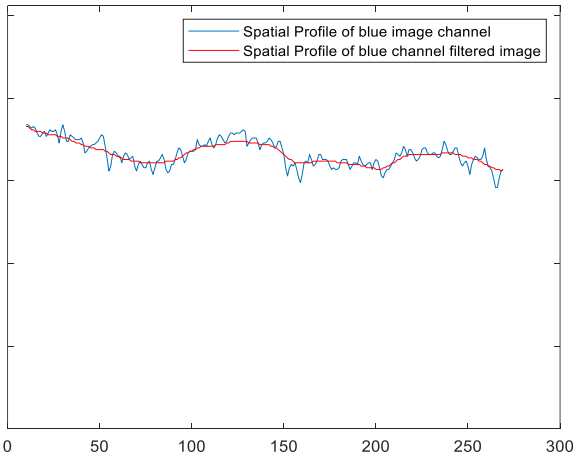

(4) RMSE=3.75

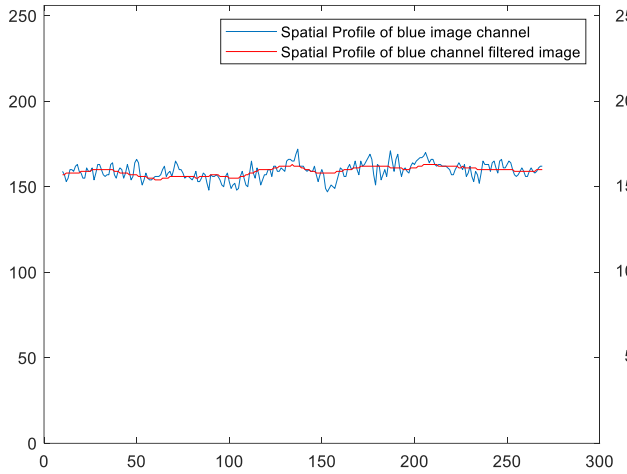

(5) RMSE=3.82

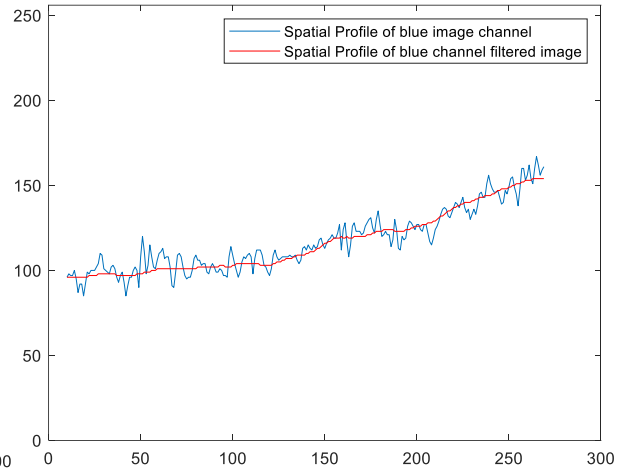

(6) RMSE=5.64

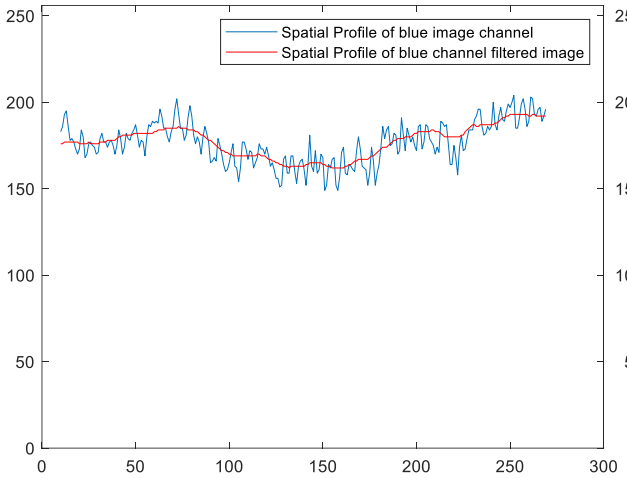

(7) RMSE=7.06

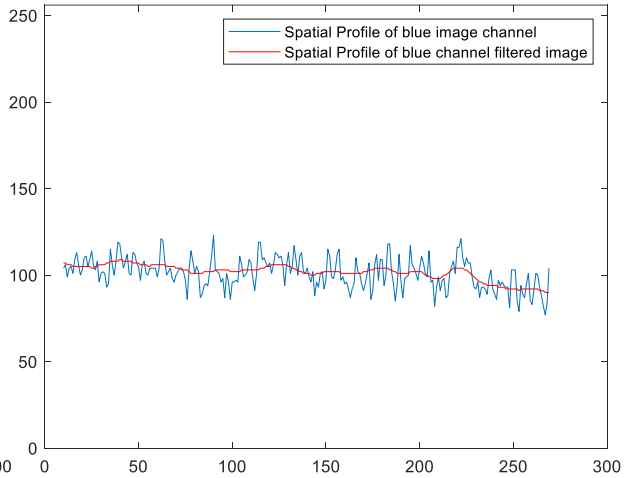

(8) RMSE=7.11

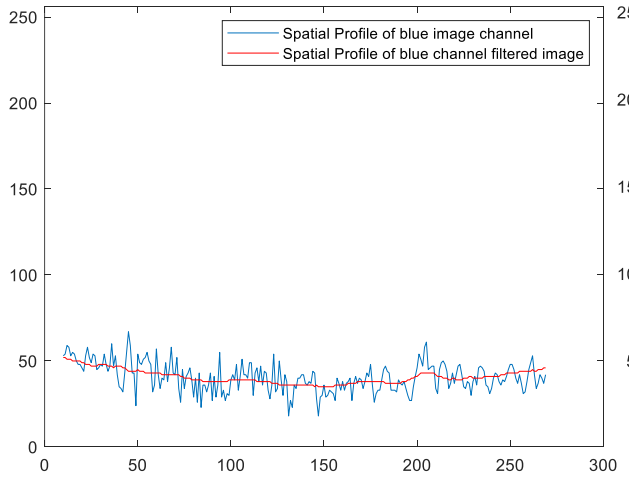

(9) RMSE=7.33

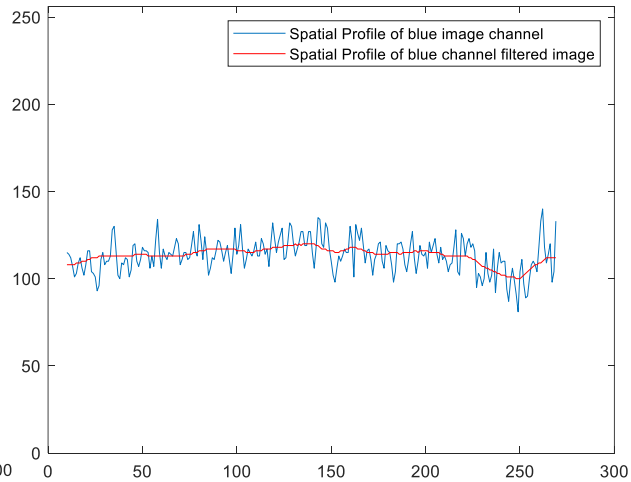

(10) RMSE=8.15

Figure 4. 2: Spatial profiles of images of Fig 4.1 with the corresponding RMSE values

Image	RMSE
1	1.64
2	2.79
3	2.83
4	3.75
5	3.82
6	5.64
7	7.06
8	7.11
9	7.33
10	8.15

Table 4. 1 RMSE values of each image of Fig 4.1

Looking at Figure 4.2, we notice that as the lesions appear on the skin, the profile of the original image (blue line) becomes denser and the values are farther apart than the profile of the filtered image (red line). This is because skin lesions create gradations in the intensity between the pixels of the images.

Verily, we see that image 1 has the lowest RMSE value. If we look carefully at all skin texture samples and compare them with each other, then this value is reasonable, because the smoothest surface is shown in image 1 and it has the best skin condition. Images 2 and 3 are the next images which have low RMSE value and differ little to each other in the decimal part, where the highest RMSE value between these two images, results from the profile of image 3. If we compare images 2 and 3, we can observe that have minimal differences between them, whereas image 3 is a little more intense than image 2.

Furthermore, the skin texture of Figure 2 seems to be very close to the texture of image 1, but if we look more closely at image 2, more skin details are beginning to appear, which also explains the difference in the value of RMSE between them.

About images **8, 9** and **10** and according to Table 4.1, we notice that they have the highest values of all, whereas the largest RMSE value is obtained by analyzing the intensity profile of Figure 10. The differences between Figures 8 and 9 are not significant, while the smallest value results from the intensity profile of Figure 8. Image 10 shows the most severe skin lesions of all, which seems to has a rougher skin surface texture than the others skin samples.

For the rest of the images from Table 4.1 and in ascending order, samples 4 and 5 are obtained, followed by 6 and 7. The values of the first two are very close to each other and do not differ much from the RMSE values of the smooth surfaces skin textures. Looking at the pictures above, it can be seen that they tend to be smooth surfaces, however some details of the texture are distinct, especially on image 5. The same happens with the 6 and 7 images, but their RMSE values is close to the values of the skin surface textures with skin lesions, which apparently these textures tend to start to have a better visible deterioration.

4.1.2 Results from Gray Level Co-occurrence Matrix Method

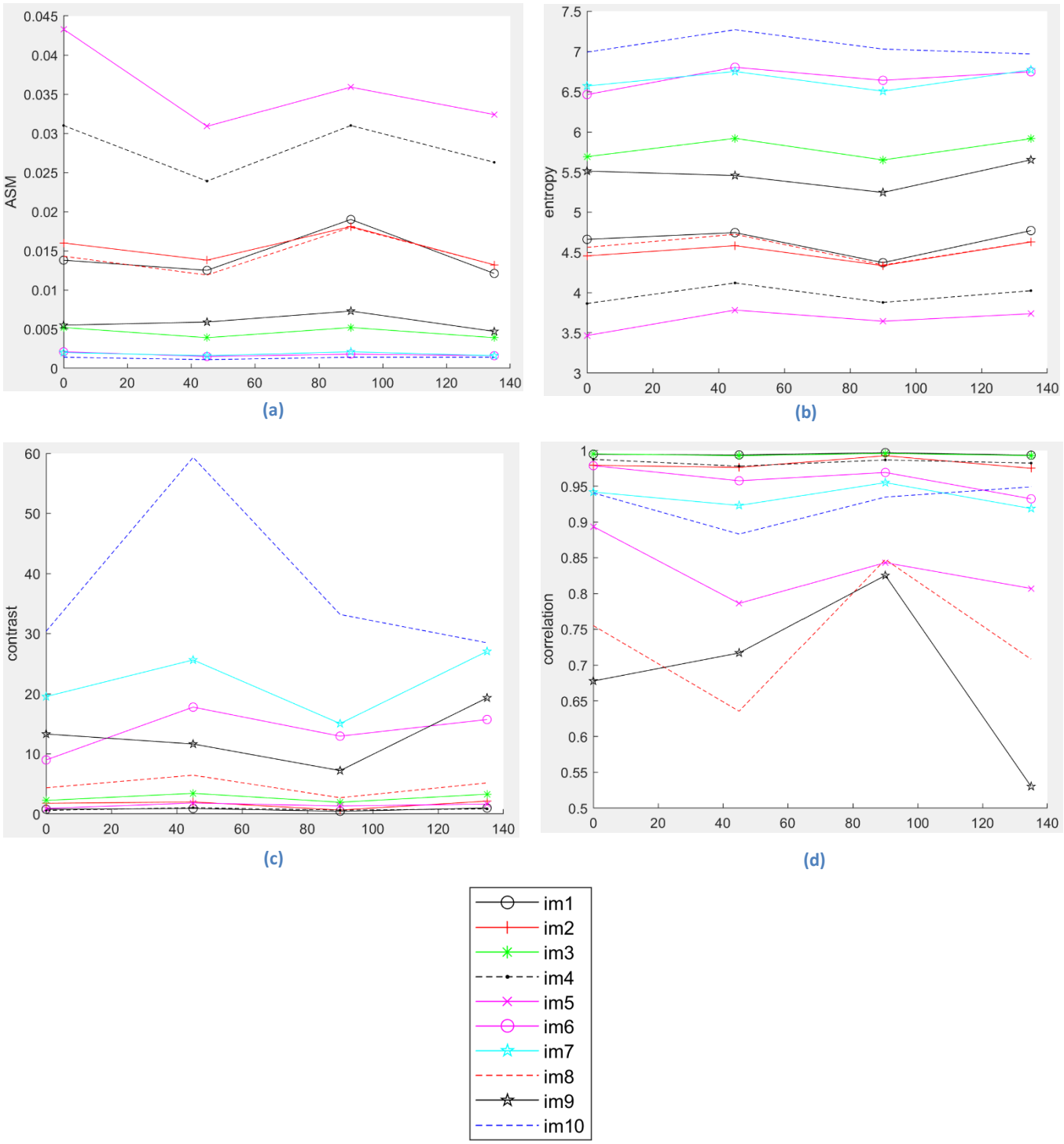

Figure 4. 3: The relation of Characteristics Parameters

Fig. 4.3(a) shows the calculations of angular second moment, which was shown in the 10 images of Fig. 7 in the 0°, 45°, 90°, 135°directions. As can be seen from the Figs. 4.3a)-(c) image 5 has the maximum ASM value of which the skin texture situation is not the best, while image 10 has the minimum ASM value of which the skin texture situation is the worst indeed.

Angular second moment (ASM) welly reflects the uniformity of skin texture coarseness and gray distribution (see 3.2.2). Moreover, image 4 has also a high ASM value, but both skin textures of images 4,5 show an average skin texture condition but quite close to textures with a smooth surface, which does not justify the high ASM values of them. Respectively, the ASM values of images 6 and 7 have a small deviation from the ASM value of 10, which is not reasonable, because their skin surface textures are much better than the texture of image 10. On the other hand, image 1 whose texture is obviously the best, its ASM value should be the highest. On the contrary, as shown in Fig 4.3(a), the ASM value of image 1 suggests that it belongs to those who should represent an average skin texture and is between images 2 and 8 ASM values. The value of Figure 8 tends to be low which means better texture than 9 and 10 which is valid, but also similar texture than 2 which belongs to smooth surfaces. Furthermore, energy value of image 3 is lower than value of image 2, which is correct because skin surface texture of image 2 is better than image 3, but energy value of image 3 is very low and close to the value of image 10, whose skin surface texture is the worst. One other thing that does not exists, is the energy value of image 7 which is very close to the value of images 10 and 6, and lower than the value of image 8 and it means that its skin surface texture is similar to the skin surface texture of image 6 which is true, but it is not similar to texture of image 10 and it has neither better surface texture than image 8.

Fig. 4.3(b) shows the calculation results of entropy in the directions of 0°, 45°, 90°, 135°. The entropy indicates the randomness of skin image gray distribution. The better skin condition is, the less value of entropy is. Images 4 and 5 have the two lowest values, but they do not belong to those with the best texture. The highest values are obtained by image 10 which has the worst skin surface texture, indeed. Entropy values of images 6 and 7 are close enough each other as well as their textures, but are also close enough to the entropy value of image 10 with the worst surface texture, which does not exists. The entropy values of images 1, 2 and 3 show that the condition of the skin is neither smooth nor so altered, while they are included in the images with a smooth skin surface, compared to the rest. Finally, for images 8, 9 the entropy value of image 9 is quite higher than image 8, but their textures is similar to each other, while entropy of image 8 is close enough to image 2 which has a much better skin surface texture.

The results of contrast and correlation are shown in Figs. 4.3 (c)-(d). Correlation reflects the similarity of skin texture in a certain direction. The experiment shows that if the contrast of skin image is small, its correlation will be big. However, if contrast is big, its correlation will be small. In addition, the diagram of contrast shows a large dissimilarity in the curves for each image, which may affect the results.

4.1.3 Results from FFT-Butterfly Method

As has already been mentioned, this method based on the geometrical characteristics of the skin surface texture (see 3.2.4). Extrinsic aging occurs in addition to intrinsic aging as a result of sun and environmental damage. Extrinsic aging shows up as thickening of the cornified layer, precancerous changes such as lesions called actinic keratosis, skin cancer, freckle and sun spot formation, and exaggerated loss of collagen, elastin, and GAGs. Alone or in concert, these processes give the skin the appearance of roughness, thin skin and deep wrinkles.

Wrinkles and fine lines that appear to the skin give a geometric characteristic to the skin surface texture, such as the skin surface microrelief.
However, this method, using our own samples, does not satisfy the algorithm, as it is not possible to convert images to binary images, due to the fact that there are no sharp changes in the surface of the skin compared to microscopic samples (see Fig. 3.7). The algorithm was also performed by omitting the conversion step to binary, but even in this case, there were no significant results that satisfied the relationship between the skin surface texture as age increased. The results obtained from the Fourier transform algorithm and the centered Spectrum after shifting the zero-frequency component of images in Fig. 4.1 are presented below.

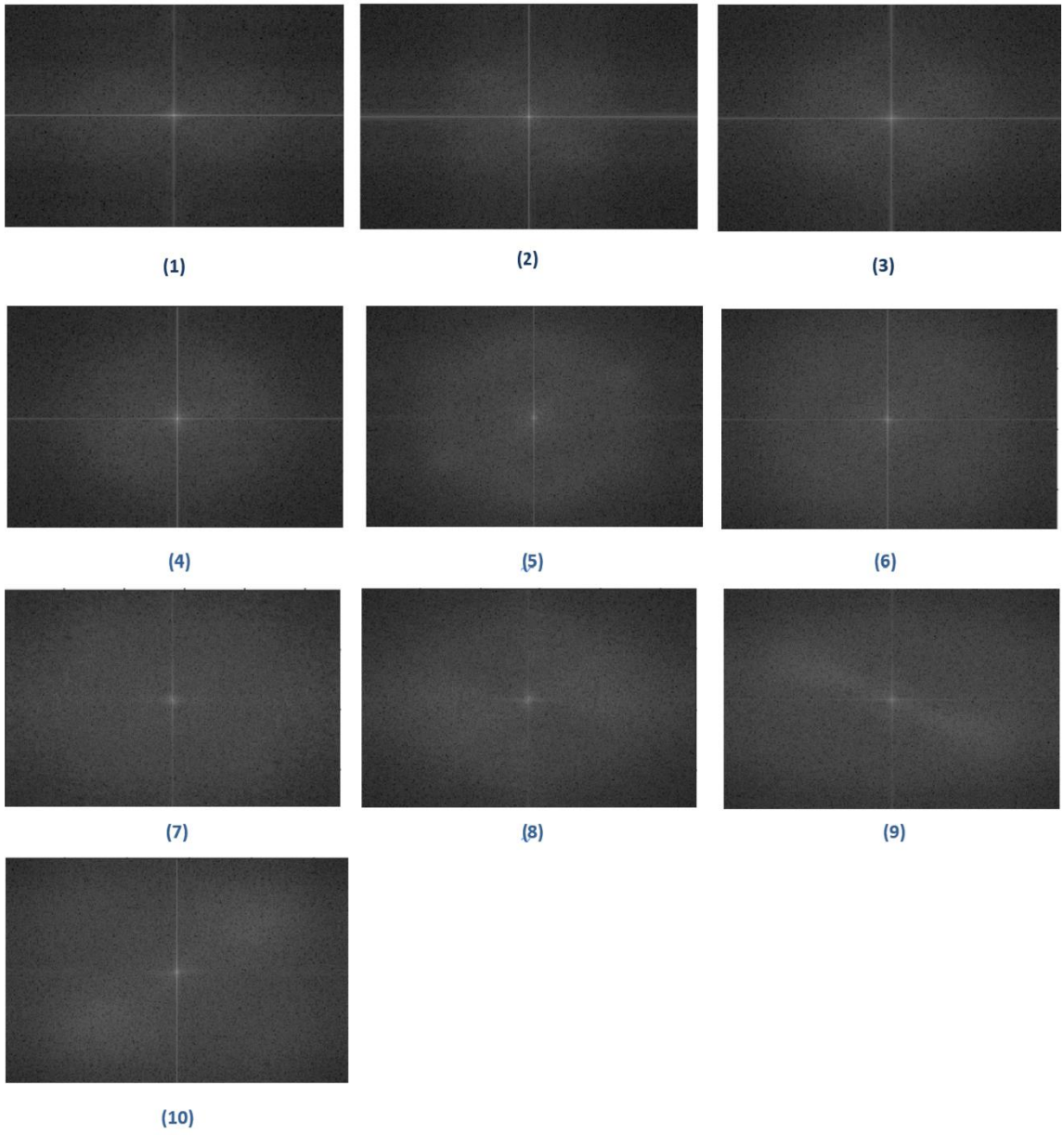

Figure 4. 4: Fast Fourier Transform of images of Fig 4.1

The parameter, called ‘‘irregularity skin index’’ (ISI), was identified from FFT. ISI was calculated by FFT in two different directions (referred to the x and y axis of the diagram of the FFT and named, respectively, ISI_{wx} and ISI_{wy}). ISI_{wx} and ISI_{wy} (irregular skin index of the wx axis and the wy axis) represent the integrals of areas delimited by the two curves derived from density of pixels in the wx and wy axes. Table 4.2 shows the results of ISI_{wx} and ISI_{wy} indexes.

Image	ISI_{wx} (x1000)	ISI_{wy} (x1000)
1	9.69	1.48
2	9.31	1.32
3	9.97	1.52
4	1.01	1.53
5	1.08	1.77
6	1.16	1.64
7	12.17	1.85
8	1.16	1.77
9	1.21	1.86
10	1.23	1.89

Table 4. 2: Results of Irregularity Skin index

From the results obtained from Table 4.2, it is obvious that the irregularity skin indexes of the wx and wy axis are not correlated with the skin condition. ISI_{wx} has large values on images 1, 2 and 3 and image 7 which has neither the best nor the worst skin condition, has the maximum value of ISI_{wx}. ISI_{wy} does not provide significant changes on its value. Therefore, there is no correlation between skin texture condition and irregularity skin index by analyzing our skin texture images. Moreover, from fig. 4.4 we can see that does not appear any pattern (such as butterfly or directional) that could be correlate the skin texture condition.

4.1.4 Results from FFT-Butterworth Filtering Method

In this case the Fourier transform is used indirectly to enhance the image with a high-pass and a low-pass Butterworth filter in the frequency domain. High-pass butterworth filter is applied to enhance the edges of the image in order to show how rough is the skin surface texture, while the low-pass butterworth filter is applied to remove high frequencies and to decrease the contribution from the skin’s curvature (see 3.2.4). The split in two frequency components was done through a low-pass digital Butterworth filter with spatial frequency 7.
Skin texture can be determined by measuring the width of the intensity distribution (histogram) of the image, which is proportional to the roughness of the sample.

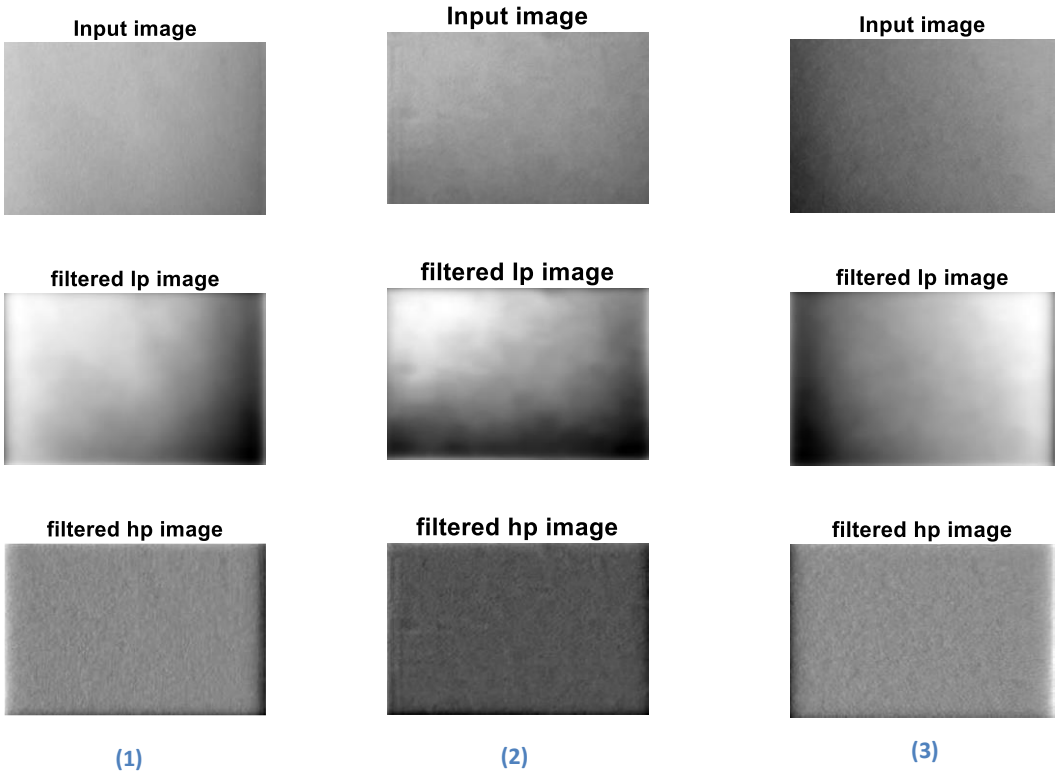
Input image
Input image
Input image
filtered lp image
filtered lp image
filtered lp image
filtered hp image
filtered hp image
filtered hp image
(1)
(2)
(3)
Input image
Input image
Input image
filtered lp image
filtered lp image
filtered lp image
filtered hp image
filtered hp image
filtered hp image
(4)
(5)
(6)

Input image

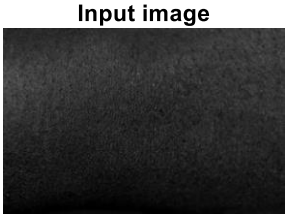

filtered lp image

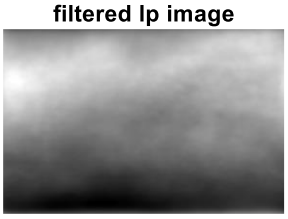

filtered hp image

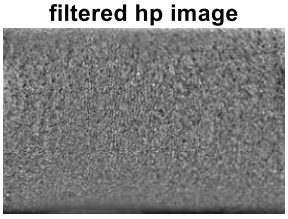

(7)

Input image

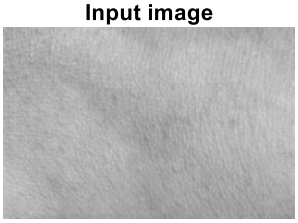

filtered lp image

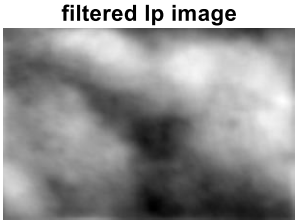

filtered hp image

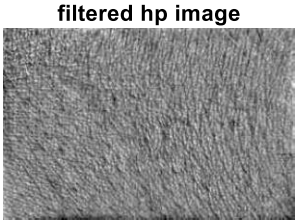

(8)

Input image

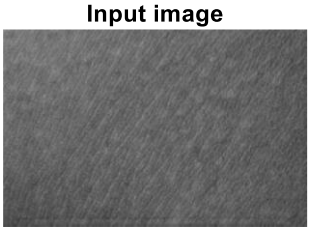

filtered lp image

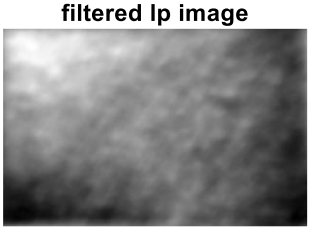

filtered hp image

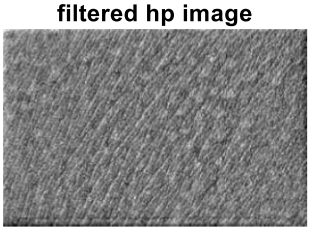

(9)

Input image

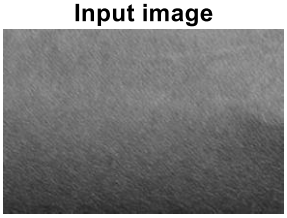

filtered lp image

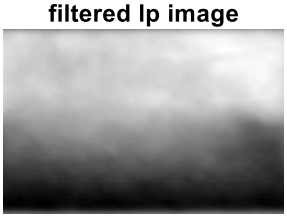

filtered hp image

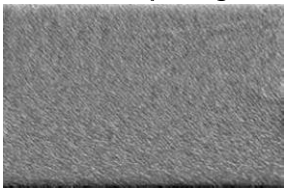

(10)

Figure 4. 5: blue channel, low pas (lp) frequency component and high pass (hp) frequency component of each image of Fig. 4.1

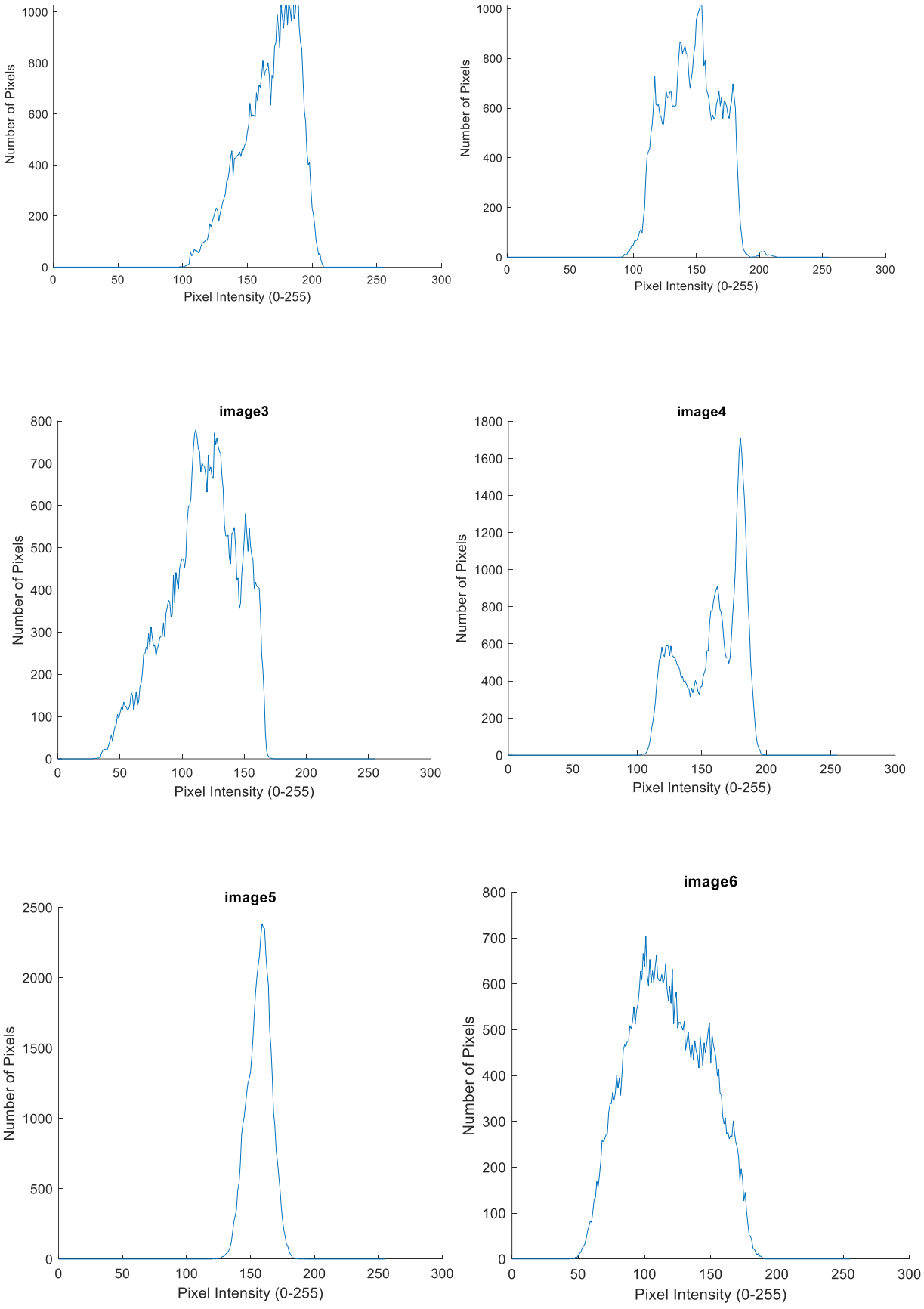

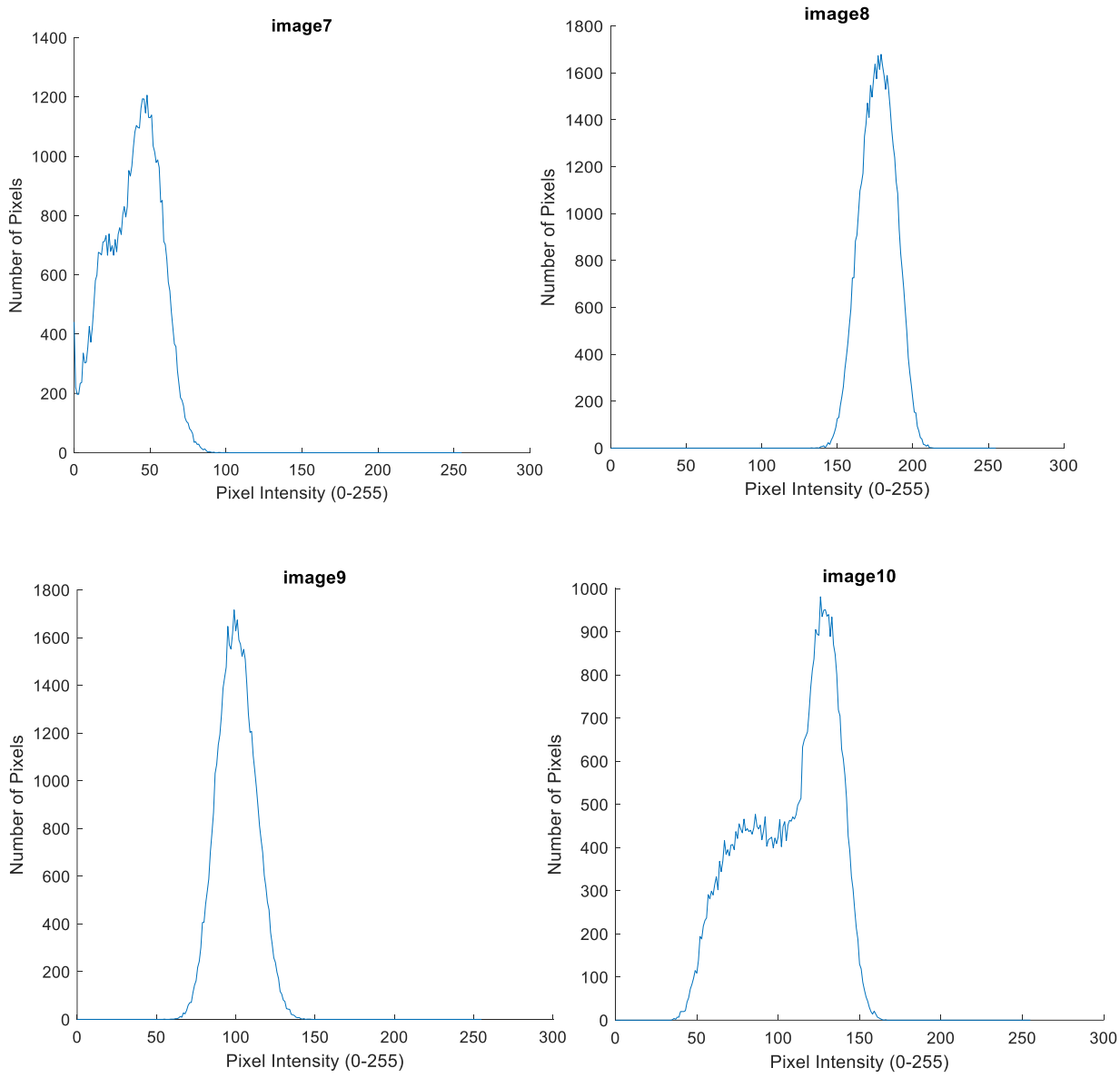

Figure 4. 6: The pixel intensity distribution of each image of Fig. 4.1

Fig 4.5 shows above are two of the results of this algorithm. From these, it seems that image 3, which has a better texture, which is also observed from the high frequency component of the filtered image, has a larger width of intensity distribution than image 8. This should not happen, as a smooth skin surface texture image does not show significant changes in gray levels, which means that the intensity value of gray levels in each Pixel is very close to its neighbors, so the width of the histogram will be smaller. In addition, in the low-frequency component depict strongly the shadows that exist in each image and does not decrease the curvature of the skin. According to the rest of samples of Fig. 8, there is no correlation between them, as images with an altered texture has a smaller width of the pixel intensity distribution than images with a smooth surface.

4.1.5 Conclusions

From the results obtained from each of the above methods, the following conclusions can be drawn:

- The only method whose results are related to the condition of the skin and quantify it appropriately (better skin surface texture smaller RMSE), is Image Spatial Profile in Relation to the Smooth Method. Another important advantage of this method is that it is not affected by shadows which is likely to be present in a digital image, so it makes it more flexible compared to other methods. Another important benefit is that this method can be easily implemented in real-time on-line applications.

- The next best method is the GLCM method, which gives us more information about the skin texture, but is quite affected by the contrast of images or shadows that may be present in them and creates false results.

- The method used by the FFT & Butterwort filter responds better concerning to skin roughness and requires the same way of taking digital images for their comparison, as the results are quite affected by the contrast. In addition, it is limited to areas of the skin (especially on the face) where roughness is visible and becomes more starkly as age increases.

- FFT-Butterfly method is limited to taking digital images that show the microrelief of the skin surface texture (mainly under a microscope).

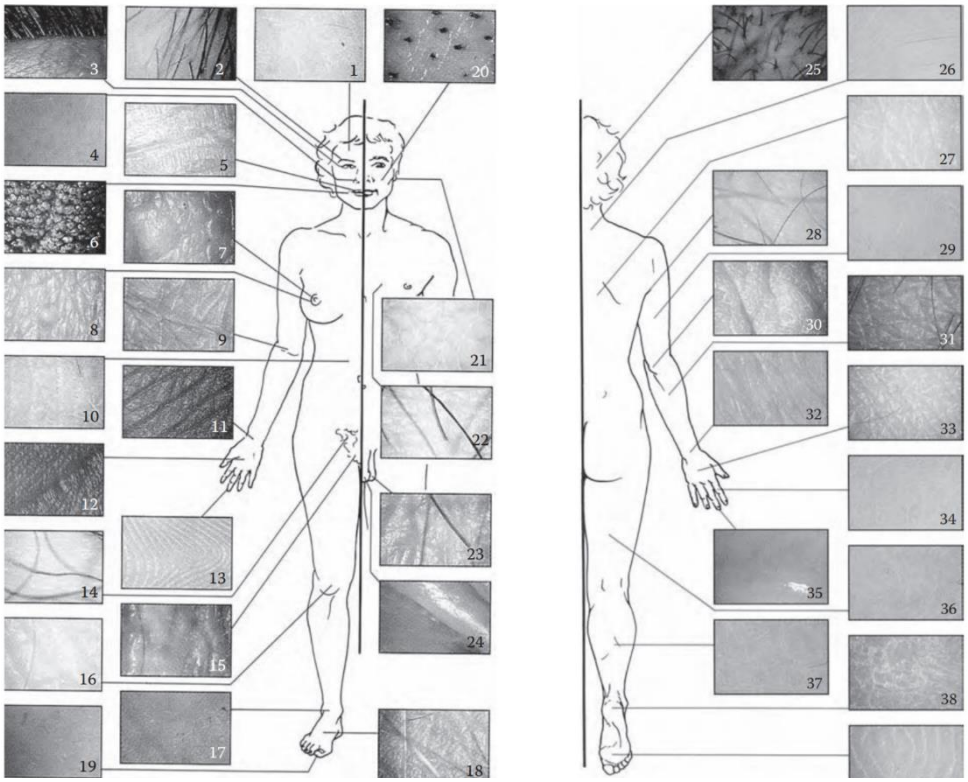

Figure 4. 7: Map of the regional differences of skin texture.

Given all of the above, the best way to quantify skin texture is through the variable RMSE, which is extracted from spatial profiles of the blue channel of the image and its smoothed. As the texture of the skin changes over time or is affected by exogenous factors as mentioned above and thus changes appear on it, this value increases. In addition, this method is flexible for the area under medical examination, because while the skin with the naked eye seems to have the same pattern, but observing it with a magnifier or a simple dermoscope, can easily see that the pattern is different in some areas of the skin as shown in Fig 4.6.

	Our Proposal Method	**GLCM**	**FFT-ISI index**	**FFT-Butterworth filter- Histogram**
Correlation with skin texture condition	✓	✗	✗	✗
Not Affected by brightness gradations	✓	✗	✗	✗
Measurements in all types of skin aging texture features	✓	✓	✗	✗

Table 4. 3: Comparison of methods

Part 5: Hyperspectral Analysis of Skin Texture

5.1 Introduction

Visual observation has an important role in dermatology as the skin is the most visible organ. This makes dermatology a good candidate for utilizing digital imaging and automatic diagnostic tools. Hyper-spectral imaging is now one of the most developed methods of visible light imaging. It enables to acquire data of an object in any spectral range set in the camera. This method is entirely non-contact and non-invasive, and measurements can be carried out remotely. With these advantages, hyper-spectral cameras are used in many fields of technology and medicine. In particular, they are used in dermatology. The issue of dermatological research concerns spectral skin analysis in almost all cases.
The surface of the body is an excellent area for deployment of optical research methods, and HSI technology is being applied in ever more applications in dermatology for non-invasively targeting cancer detection, skin oxygenation mapping for diabetic ulcers, spectral unmixing of fluorescently labeled antigens, and more.

5.1.1 Tissue Optics Principles

The human skin presents a complex heterogeneous medium, where the blood and pigment content are spatially distributed variably in depth. The human skin is named cutis, and is composed of two layers; a top layer called epidermis and a bottom layer called dermis. Below dermis, there is a subcutaneous fat layer.
Information about skin physiology, morphology, and composition can be obtained non-invasively by optical imaging methods. When light interacts with tissue, it is usually altered in some way before being remitted and detected by an image sensor. Photons can be scattered because of the refractive index fluctuations on a microscopic level by collagen fibers or by membranes, have their polarization altered after multiple scattering events, or be absorbed by molecules such as hemoglobin or melanin.
The epidermis varies in thickness from 0.3 mm to 1.5 mm, and consists of a multilayer plate epitel. Almost all of the cells in epidermis, around 90%, are keratinocytes. The epidermis is further divided into layers called strata. These layers are the basale layer, the spinous layer, the granular layer and the corneum layer, as seen in Fig. 5.1. Melanin is found in the epidermis in the form of red/yellow pheomelanin and/or brown/black eumelanin that absorbs very broadly in the visible spectrum with higher values for shorter wavelengths.

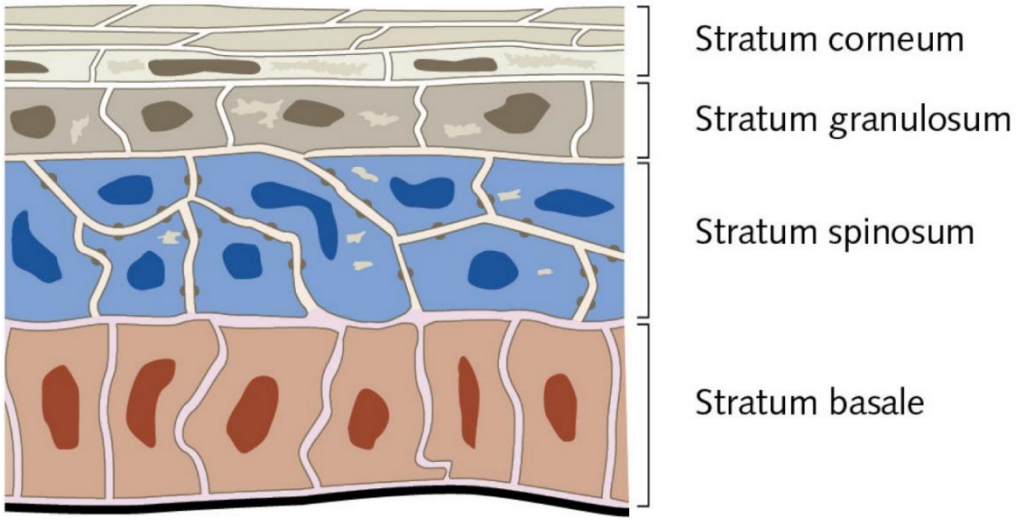

Figure 5. 1: The composition of epidermis

The dermis, which is located below the epidermis, varies in thickness from 1.4 mm to 4 mm. Dermis consists of collagen and elastic fibers, and is divided into two layers, where the lower is called the reticular dermis and the upper is called the papillary dermis. An illustration of the composition of dermis can be seen in Fig. 5.2. The layers are composed of connective tissues, blood vessels, and nerves. In the blood cells there are several natural chromophores, primarily hemoglobin, which absorbs blue and green light and gives blood its reddish color. Other chromophores present can include bilirubin and _-carotene that when found in the dermis contribute to the yellowish or olive tint of human skin. Fig. 5.5 displays the absorption spectra of major skin constituents that have a distinctive spectral absorption signature.

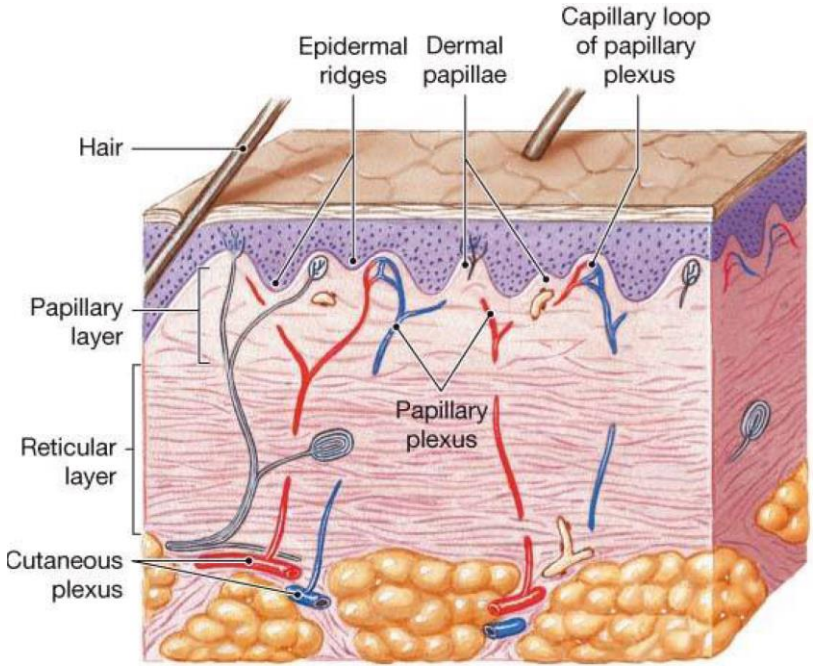

Figure 5. 2: The composition of dermis

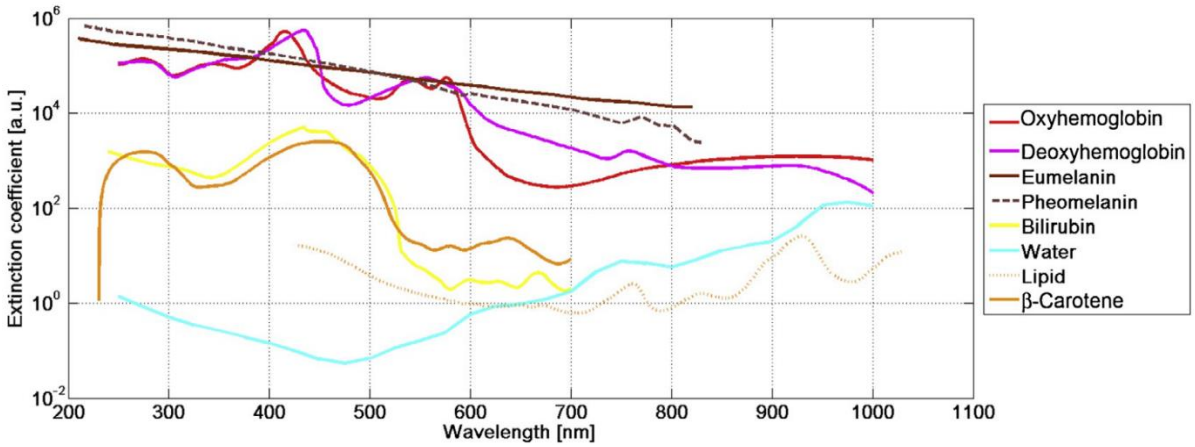

Figure 5. 3: Absorption spectra of skin constituents

Light entering tissues can also have its wavelength distribution shifted by interaction at the atomic or molecular levels, producing fluorescence or Raman signals. Interpreting these changes can provide diagnostically useful information about the underlying structure of the tissue, provided that there is a plausible biological rationale for the change. Changes in the spectral characteristics in different wavelength regions produce a distinguishable spectral signature that reflects the underlying biology. Spectral imaging technology has a unique capability for skin characterization because it can take advantage of the spatial relationships among the different tissue absorption spectra in a neighborhood. Spectral data cube analysis can incorporate complex spectral-spatial models that can provide more accurate classification of image features specific to a targeted disease. The technology unlocks new capabilities in medicine by which spatial and functional relationships among biologically active molecules can be observed, helping to noninvasively identify and quantify changes in living organisms, and enhancing histopathological and fluorescent biomarker image analyses to improve biological knowledge of diseases.

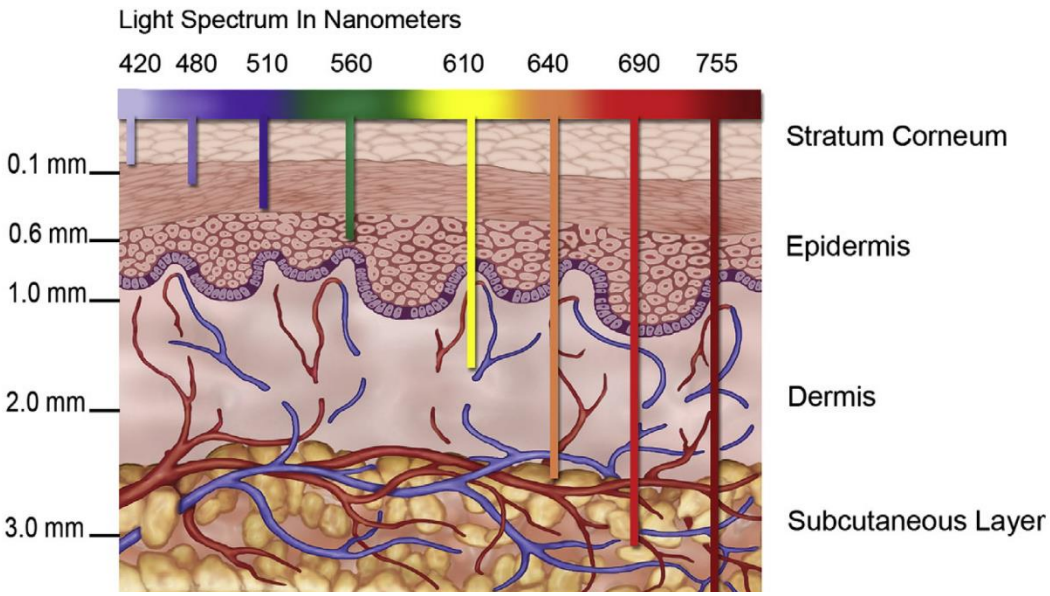

Figure 5. 4: The penetration of light of different wavelengths in the skin

The penetration depth of light into biological tissues depends on how strongly the tissue absorbs and scatters light. High melanin concentration at the topmost layer of skin (epidermis) absorbs light in the ultraviolet (UV) and visible range, leading to low penetration depth for wavelengths shorter than 600 nm. In the wavelength range from 600 to 1300 nm, skin has sufficiently weak absorbers to permit significant light penetration. Because of this characteristic, this wavelength range is often called the therapeutic window. Fig. 5.6 shows a schematic of light penetration depth at different wavelengths for human skin.

5.1.2 Spectral Imaging Technique for Assessing Skin Aging Progress

Aging of the human hand reflects the cumulative effects of time on the properties and functions of the skin and other deeper structural components of the hand. The main changes associated with normal aging of the hands are related to skin texture changes,1 the reduction of muscle strength as a consequence of decreasing muscle mass,2 joint deformity, bone spur formation and reducing the degrees of motion of the hand and fingers,3 and nerve changes and hand motor control problems.

Establishing a direct relationship between the human hand aging process and some characteristic properties of hand structural components is essential for quantitative assessment of the aging process of a hand. Many studies have been undertaken to date, most of them being focused on skin texture analysis.
Over the years, skin texture analysis became a great focus point in scientific literature, especially for computeraided diagnosis in dermatology and cosmetic products testing. The ability of skin texture analysis to provide different skin texture features as indicators of skin aging has been demonstrated by some researchers.

Hyperspectral imaging (HSI) has the advantage to provide both spectral and spatial information about each pixel from a skin image scene. Therefore, we assume that by adding spectral information to the classical texture analysis methods that only treat gray-level spatial variations, a better characterization of skin aging could be achieved.
The primary goal of this study is to analyze the skin texture features related to wavelength using the Root mean Square Error value calculated from HSI of inside hand area between wrist and elbow at a more accurate quantitative assessment of the aging process. The main issues addressed are as follows: (1) extracting the mean RMSE values of hand skin area between wrist and elbow from hyperspectral images acquired at different wavelengths; (2) selection of the highest RMSE value in the corresponding wavelength. (3) establishing a correlation between mean RMSE value and absorption spectra of the main chromophores in human skin tissue;

5.2 Hyper-Spectral Skin texture analysis using a dermoscope

Macroscopic morphological examination of skin disorders is, besides history taking, general physical examination, and laboratory investigation, one of the pilots of the diagnostic methods in dermatology. An extension of the morphological examination is the invasive technique of biopsy taking for histopathology, histochemistry, immune-histochemistry, and autoradiographic methods.
Many imaging devices have been developed for skin texture analysis such as VISIA SYSTEM (Visia Complexion Analysis, Visia-CR, Canfield Imaging System) [15], 3D Lifeviz Micro (QUANTIFICARE INC. (US)) [16], Clarity 2D & 3D Research Systems (BrighTex Bio-Photonics) [17] and Antera 3D (Miravex Limited, Ireland) [18]. However, they have disadvantages as they measure skin texture appearance using RGB images and labeling algorithms which enhance the images and show the skin texture characteristics using different colors depending on the degree of damage. Moreover, more of them are not portable devices and capture images only from face area and analyze specific features, such as only the depth wrinkles and curve lines, or roughness by labeling the spots that affect the smooth area.
Dermoscopy, which is a non-invasive micromorphological method, can be considered as a trait d'union between microscopic morphological investigations and invasive histological techniques. From the historical point of view epiluminescence microscopy has been used for two different applications: capillary microscopy and dermoscopy. Dermoscopy is a readily available diagnostic method, allowing us to appreciate the fine details not normally seen with the naked eye. It furnishes us with the overall detail, which is not the case in low-power scanning electron microscopy, the latter being, moreover, an elaborate and very expensive technique. The unexpected details seen with the dermoscope often give us answers regarding the pathophysiology of various skin diseases, as well as the urge to pose questions requiring further investigation. As such, the dermoscope can be applied as an objective tool in research, e.g., follow up of ultraviolet (UV)-erythema reaction, skin texture measurements, etc. With the existing techniques of UV, infrared (IR), and fluorescence photography, dermoscopy is used to apply these methods to the fine detail of the skin.
Dermoscopic photography provides the clinical instructor with a new valuable teaching aid that not only enhances what is seen clinically, but also creates a surprisingly pleasing visual image of color, shadows, texture, and form.

Skin is the main organ in which age-related changes are visible. Skin aging is a complex process that composed of chronologic (intrinsic) aging associated with people's genetics characteristics and extrinsic aging associated with ultraviolet (UV) such as brown spots, alcohol, smoking, malnutrition, and adverse environmental conditions. Skin performance impair with age and with the influence of these factors and visual beauty is lost. In fact, aging skin appears thicker, paler, and clear (translucent). Large pigments, including age spots, liver spots or liver lenses, may appear in areas exposed to the sun.
All these features of skin aging can be detected easily with dermoscopy. Measurement of skin aging with dermoscopy will give more reliable and objective results than the scales using clinical criteria. Prevention and treatment of skin aging can be measured using dermoscopy and efficacy of many therapeutic techniques can be investigated.

5.2.1 Skin texture analysis based on RGB color space

Using the Qcell Snapshot HyperSpectral Dermoscope, a sophisticated and evolving dermoscope, we collected the following images. Four of them are from the area on the inside of the hand between the wrist and elbow and two are from the facial area. It is important that the images do not contain hairs because they affect the results of the algorithm. Image processing is now done using the RMSE algorithm, as it emerged from the comparison of the results in Part 4, it is the best method to measure and quantify the texture of the skin. More specifically, in order to be more accurate and valid in terms of quantifying the skin texture, we calculate the mean RMSE value, which results from the RMSE values given to us by the spatial profiles in the horizontal, vertical and the two diagonal directions as shown in Fig 5.5. In this case, all intensity profiles of the images are derived from the blue channel of the RGB color space of the images.

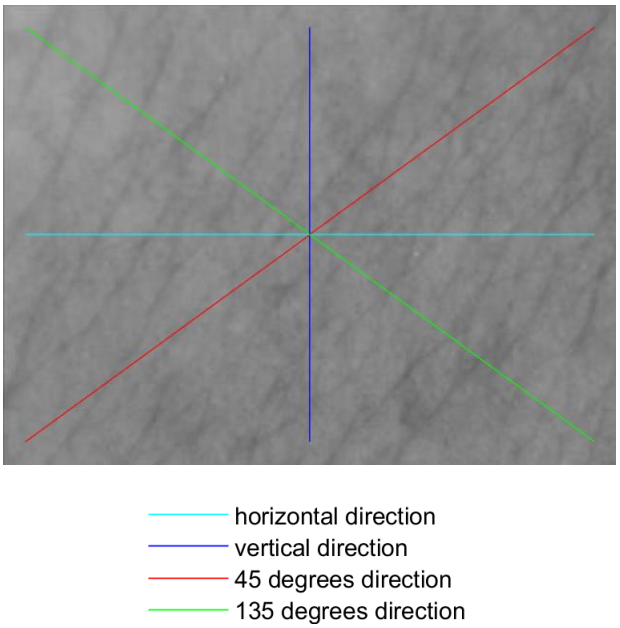

Figure 5. 5: Intensity Profiles directions

The size of the Gaussian filter which is used to blur the images is hsize=30 with sigma=16 on 292x392 image size. Comparison of the skin samples is achieved separately for those taken from the face's area and inside of the hand between the wrist and elbow area, as the skin pattern observed with a dermoscope varies depending on the area of the body, as previously reported.

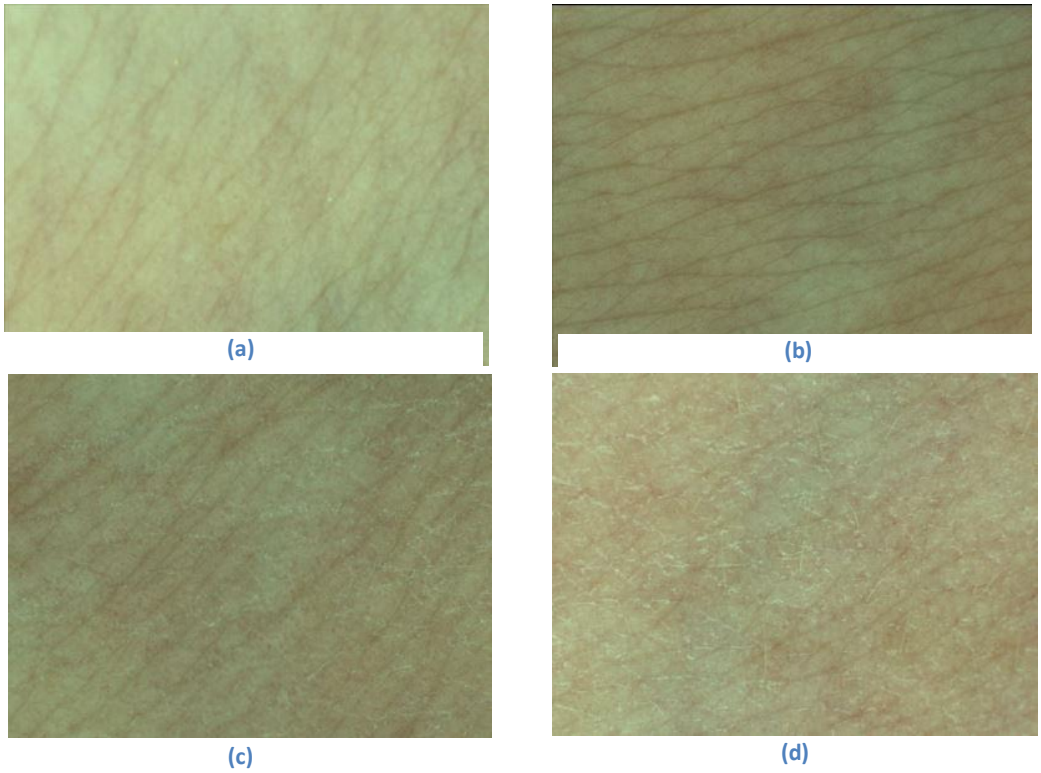

Figure 5. 6: Skin texture from inside of the hand between the wrist and elbow area

Image	RMSE values in all directions				**Mean RMSE**
	0^o	45^o	90^o	135^o	
a	4.23	4.44	4.25	4.37	4.32
b	5.14	5	4.81	5.09	5.01
c	5.23	5.46	5.47	5.66	5.45
d	6.61	5.86	5.77	6.27	6.13

Table 5. 1: Analytic results of RMSE values (hand area)

According to Figure 5.2, image (a) is the best one of the skin situation among these four images, following by image (b) while the skin situation of image (d) is the worst. More specifically, in Figure 5.2.b we observe that the fine lines appear strongly in relation to the previous one while in relation to the next ones it maintains a smoother texture. In image (c) the skin appears drier while it also shows some white signs. The same holds for image (d) in which the white signs are much more noticed. The table 5.1 shows that the mean PMSE value of the images increases from images (a) to (d) which is completely related to the condition of the skin. The mean RMSE value of image (b) is very close to the mean RMSE value of image (c), which has the largest value, and it appear fine lines and white signs which make the skin drier than skin in image (b) which contains only the fine lines.

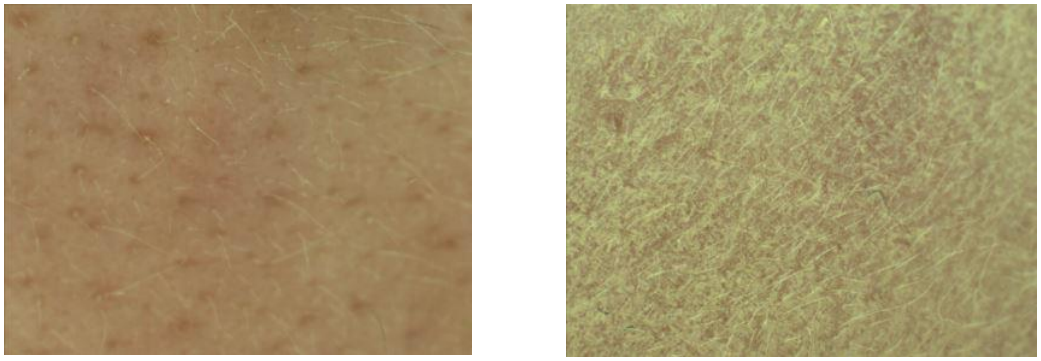

(a) (b)

Figure 5. 7: Skin texture from facial area

Image	RMSE values in all directions				**Mean RMSE**
	0°	45°	90°	135°	
a	4.13	3.49	3.49	3.76	3.72
b	9.66	9.79	10.99	9.89	10.08

Table 5. 2: Analytic results of RMSE values (facial area)

In this case, we have more obvious results, both visually and algorithmically. As shown in Fig 5.2, image (b) appears a more rough skin surface texture than image (a). Image (a) has also some signs like spots but the skin is smoother and obviously has much better skin condition. This also results from the RMSE values in Table 5, with the mean RMSE value of image (b) being much higher than the value of image (a).

5.2.2 Skin texture analysis on specific spectra

The Qcell Snapshot HyperSpectral Dermoscope has also the ability to capture image data at specific frequencies across the electromagnetic spectrum. Hyper-spectral images acquired in the visible to near-infrared spectrum may help experts and cosmetic industry to quantify and assess the aging of the human hand, by reflect the cumulative effects of time on the properties and functions of the skin and other deeper structural components of the hand.
Our aim is to evaluate which frequency band reflects the most skin characteristics and therefore the highest mean RMSE value results from it. In addition, another important observation is the establishment of a correlation between the absorption spectra of the main chromophores in human skin with the maximum mean RMSE value that results in the corresponding frequency band.
This device outputs these bands: 400nm, 460nm, 540nm, 640nm, 780nm and 880nm. We analyze skin hand area between wrist and elbow at these bands, using mean RMSE value as an assessment measure. The size of Gaussian filter is hsize=60 with sigma=25 on a 950x1500 image size.

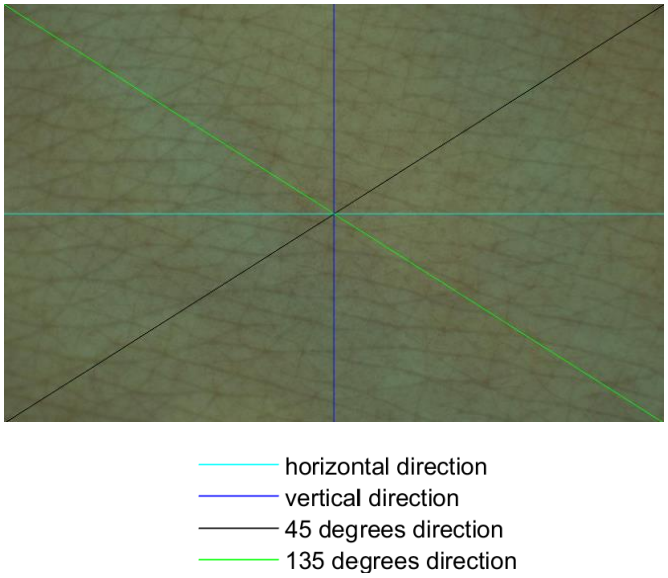

Figure 5. 8: Color Image with spatial profile directions

Figure 5. 9: Image at the frequency of 400nm

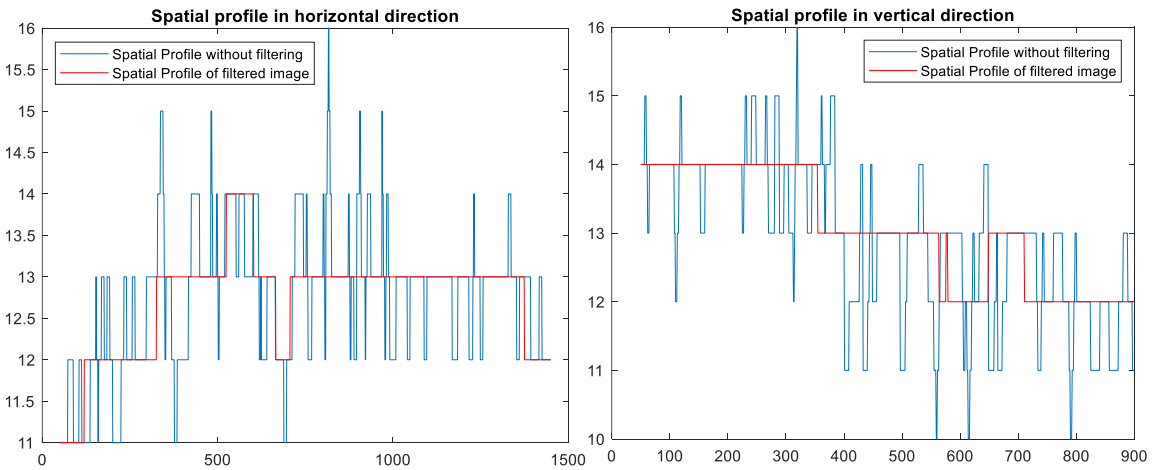

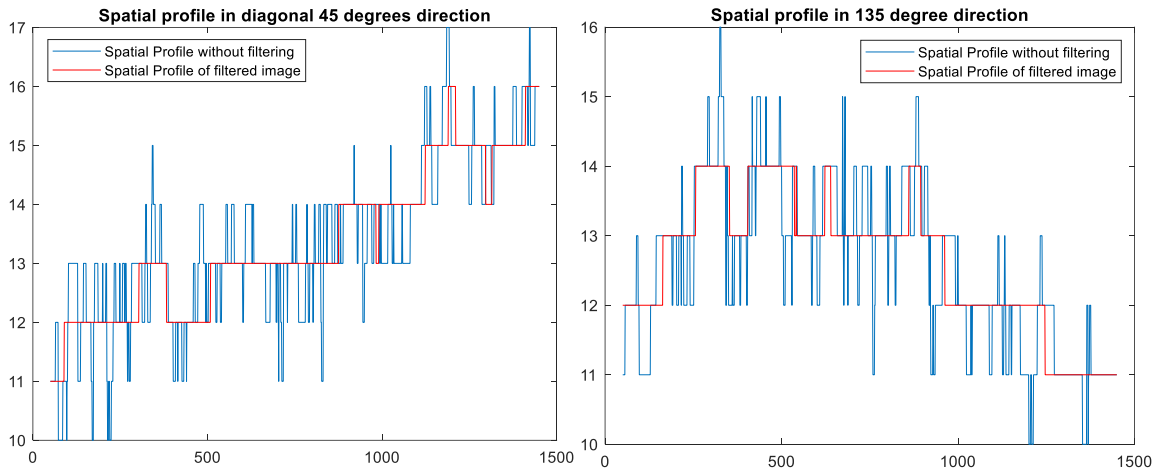

Figure 5. 10: Spatial profiles of image at the frequency of 400nm in all directions, meanRMSE=0,76

Figure 5. 11: Image at the frequency of 460nm

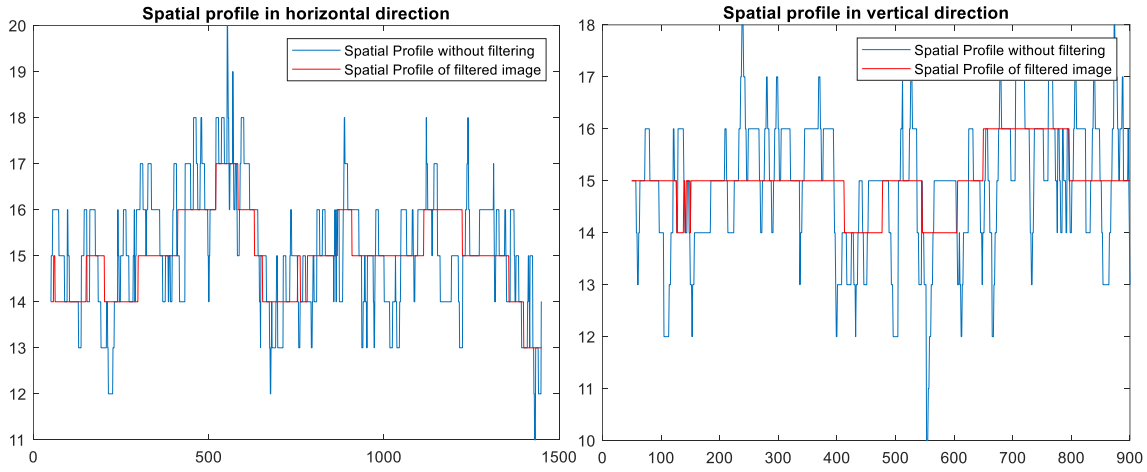

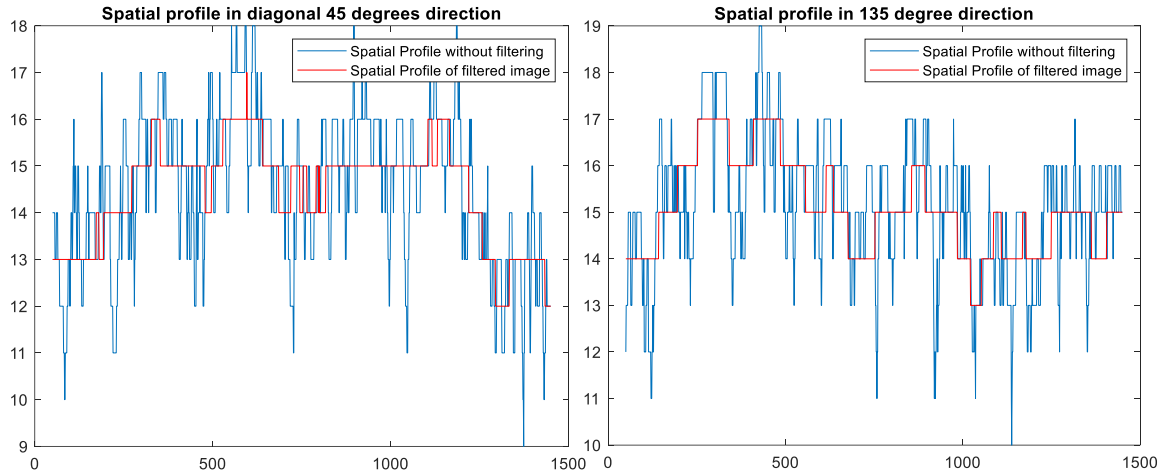

Figure 5. 12: Spatial profiles of image at the frequency of 460nm in all directions, meanRMSE=1.18

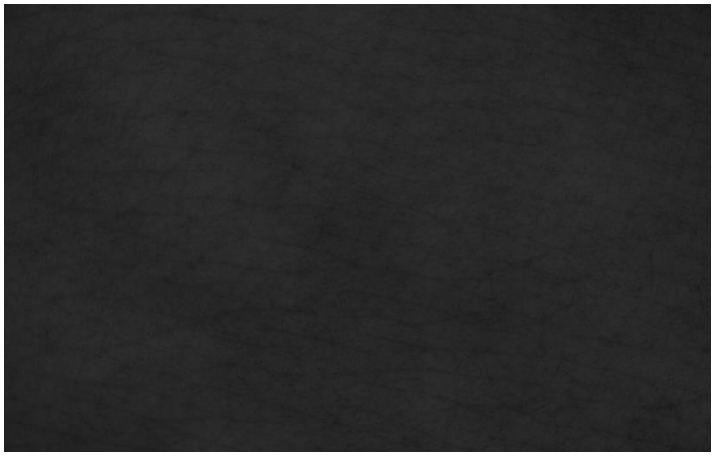

Figure 5. 13: Image at the frequency of 540nm

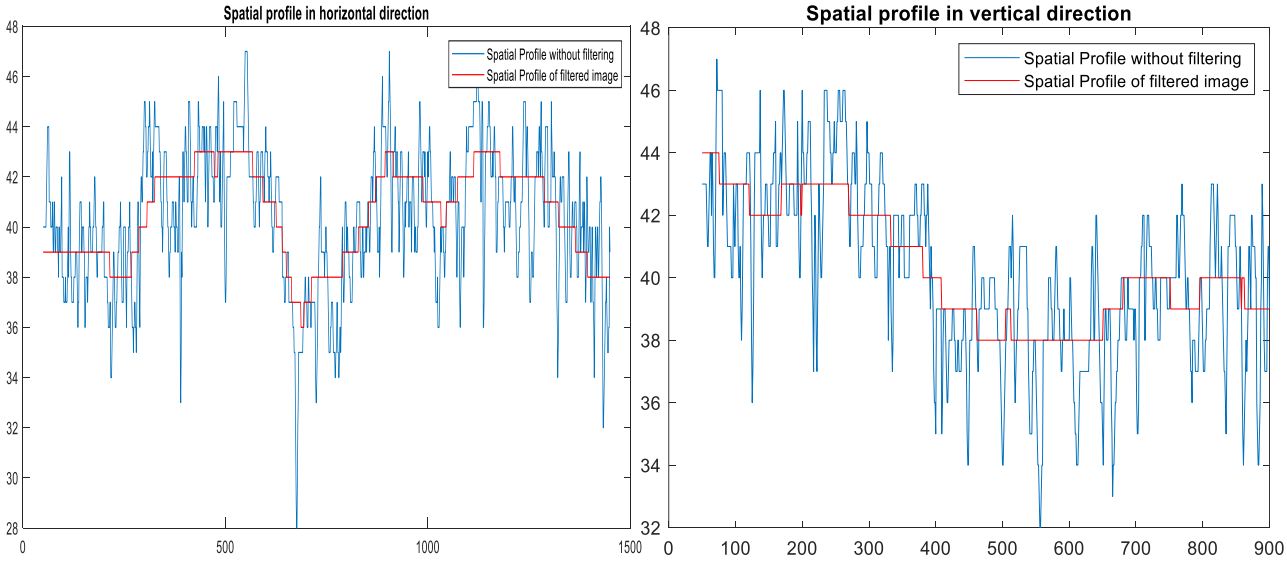

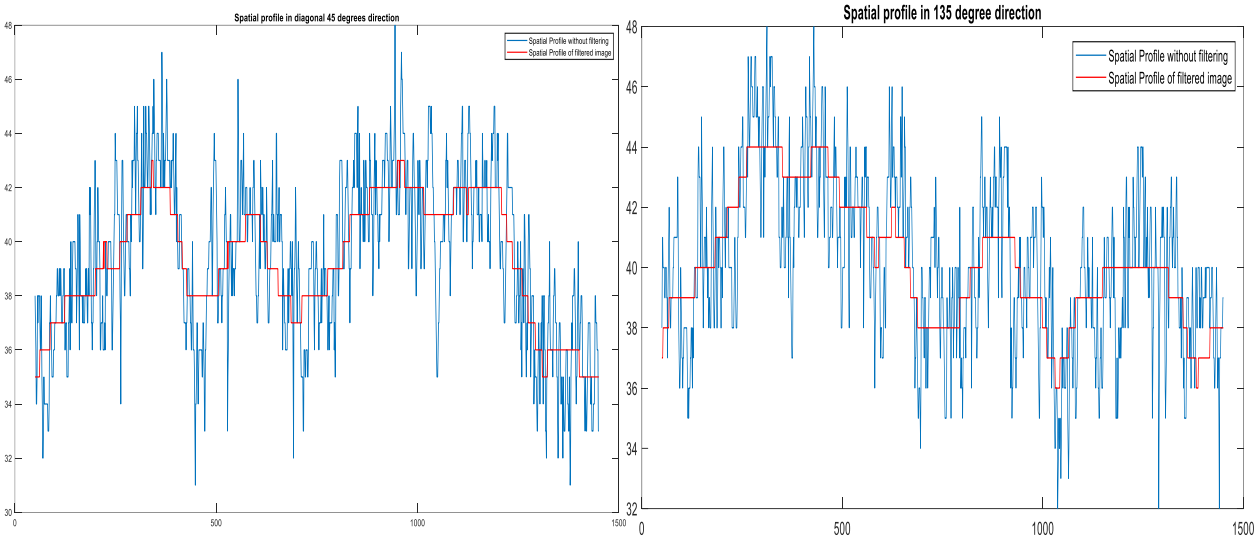

Figure 5. 14: Spatial profiles of image at the frequency of 540nm in all directions, meanRMSE=2.02

Figure 5. 15: Image at the frequency of 640nm

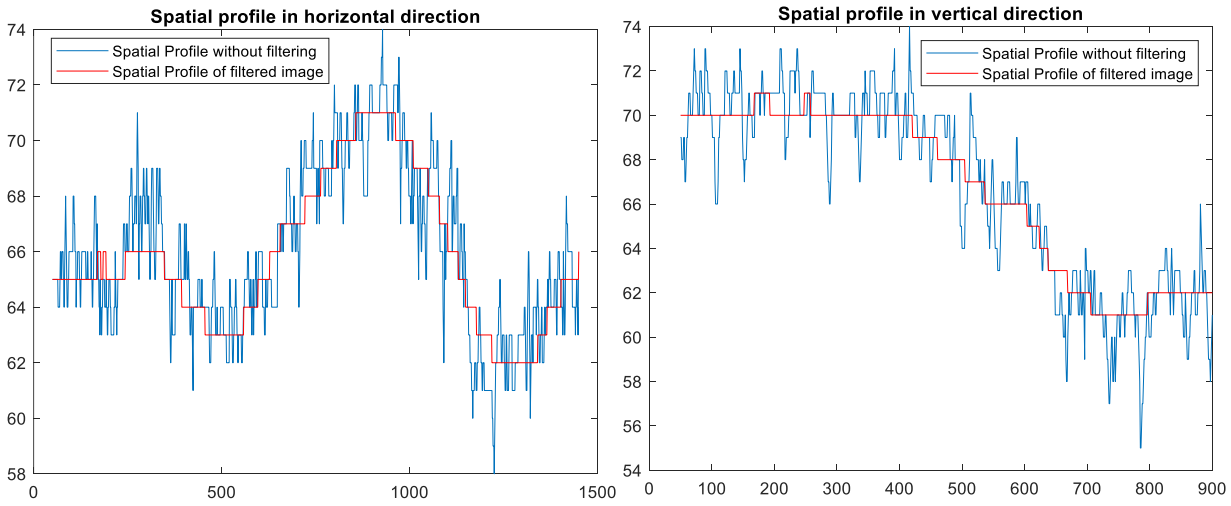

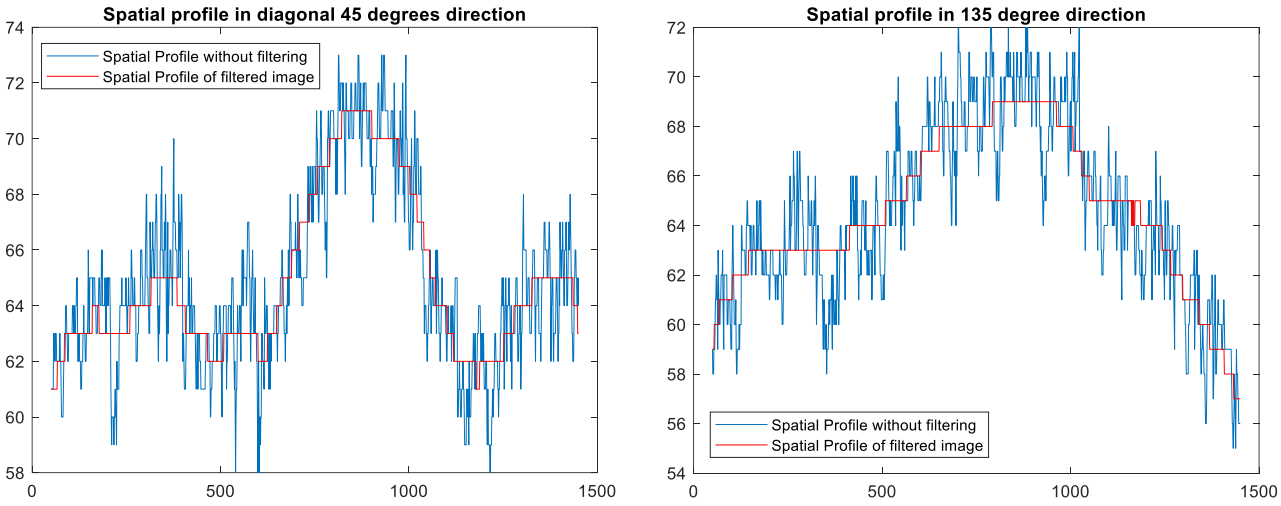

Figure 5. 16: Spatial profiles of image at the frequency of 640nm in all directions, meanRMSE=1.52

Figure 5. 17: Image at the frequency of 780nm

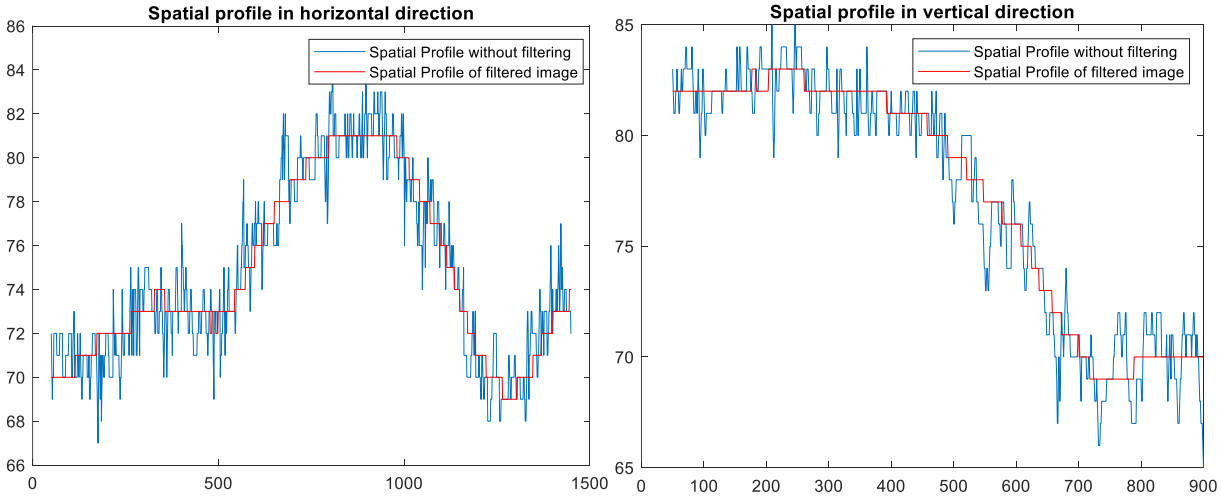

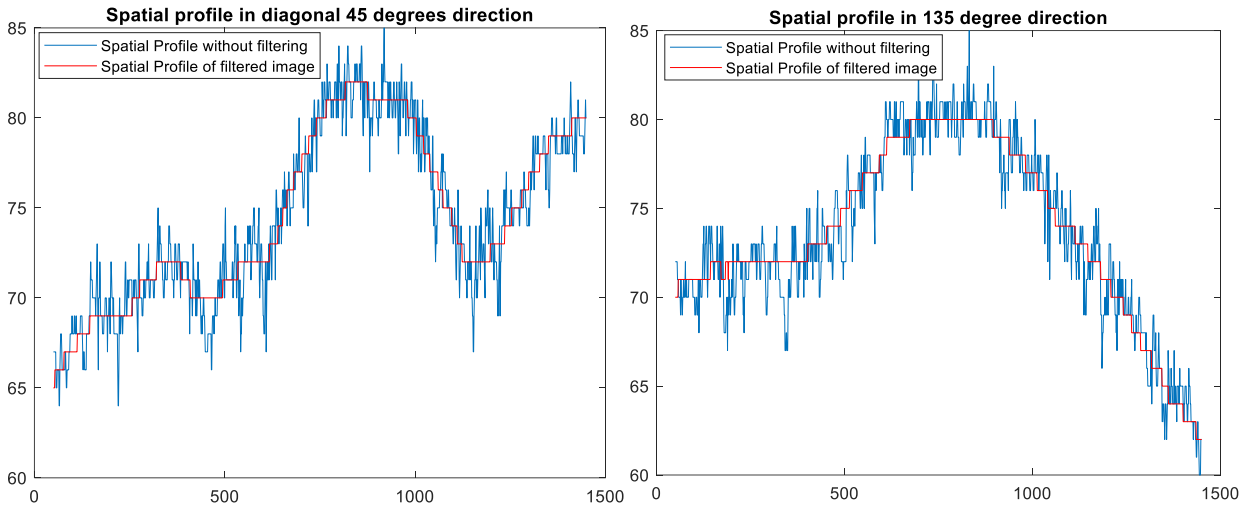

Figure 5. 18: Spatial profiles of image at the frequency of 780nm in all directions, meanRMSE=1.36

Figure 5. 19: Image at frequency of 880nm

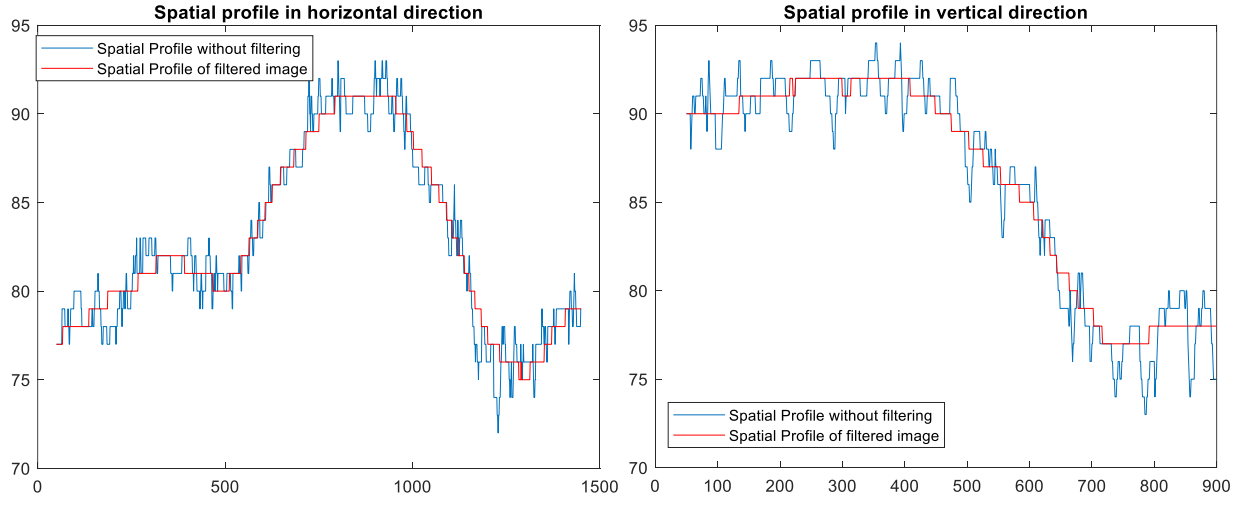

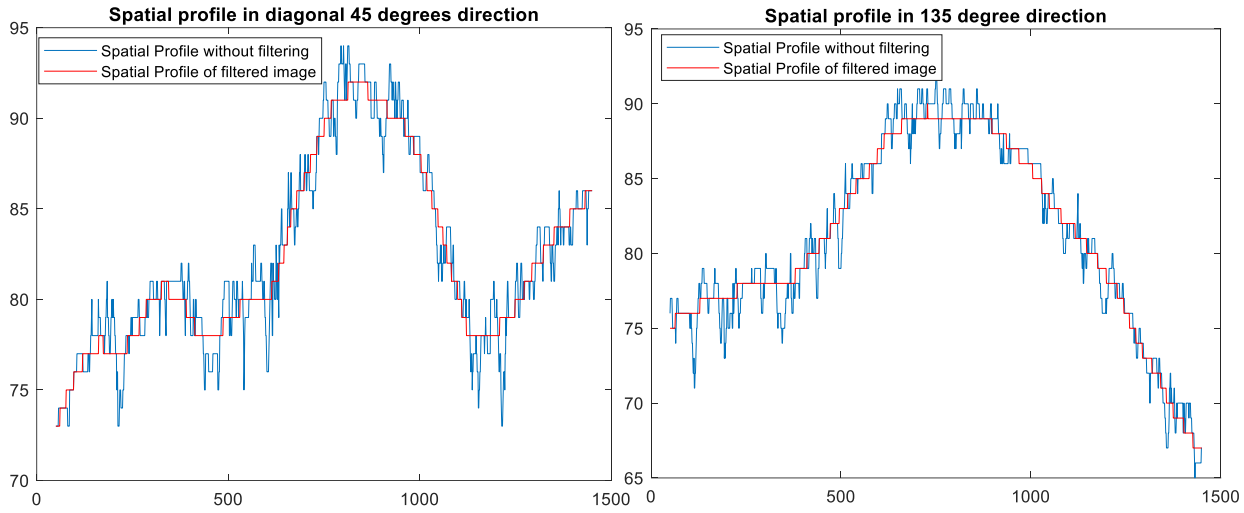

Figure 5. 20: Spatial profiles of image at the frequency of 880nm in all directions, meanRMSE=1.31

Wavelength of Image	RMSE values in all direction 0°	45°	90°	135°	Mean RMSE value
400nm	0.68	0.76	0.88	0.71	0.76
460nm	1.11	1.23	1.23	1.16	1.18
540nm	2.06	1.98	1.99	2.05	2.02
640nm	1.42	1.53	1.50	1.62	1.52
780nm	1.33	1.43	1.29	1.46	1.36
880nm	1.18	1.39	1.37	1.28	1.31

Table 5. 3: Analytic results of RMSE values of spectral images

Table 5.3 contains in detail all the values that result from the spatial profiles of the images at each spectrum, as shown in the above figures (Fig. 5.5-5.15), in all directions as well as their mean RMSE value. The maximum mean RMSE resulted by the the image in the frequency of 540 nm. Observing the spatial profiles of each spectral image in all directions, the values of spatial profiles of original image (not filtered) at the 540nm are far from the reference point (smooth image) and the spatial profiles is also denser than the profiles of the other spectral images. This justifies the maximum RMSE values in this range. In the spectra of 400 and 460 we observe smoother profiles in the original image, which means that the characteristics of the skin are not well represented in them. The same happens in the other spectra larger than 540nm. The profile curve of the original image tends to be closer to the curve of the smooth image. Therefore, it can be concluded that the spectrum of **540nm** shows extra details and potentially skin lesions of the skin texture, that create gradations in the values of the intensity of the profiles and this wavelength is associated also with better visualization of the upper

affected skin layers. Moreover, the spectrum of 540nm is very close to the maximum absorption spectrum of oxyhemoglobin (with maximum absorption peaks at 542 nm and 576 nm) and it is a fact that some degree of venous stasis is associated with aging.

5.3 Skin Texture Analysis using Hyperspectral Imaging System

5.3.1 Set up of Image Acquisition System Model

Hyperspectral image of the inside area of the hand between wrist and elbow of the participant was acquired using a staring hyperspectral imaging system consisting of an imaging spectrograph (MUSES9-HS) and containing 2x50 W halogen lamps.

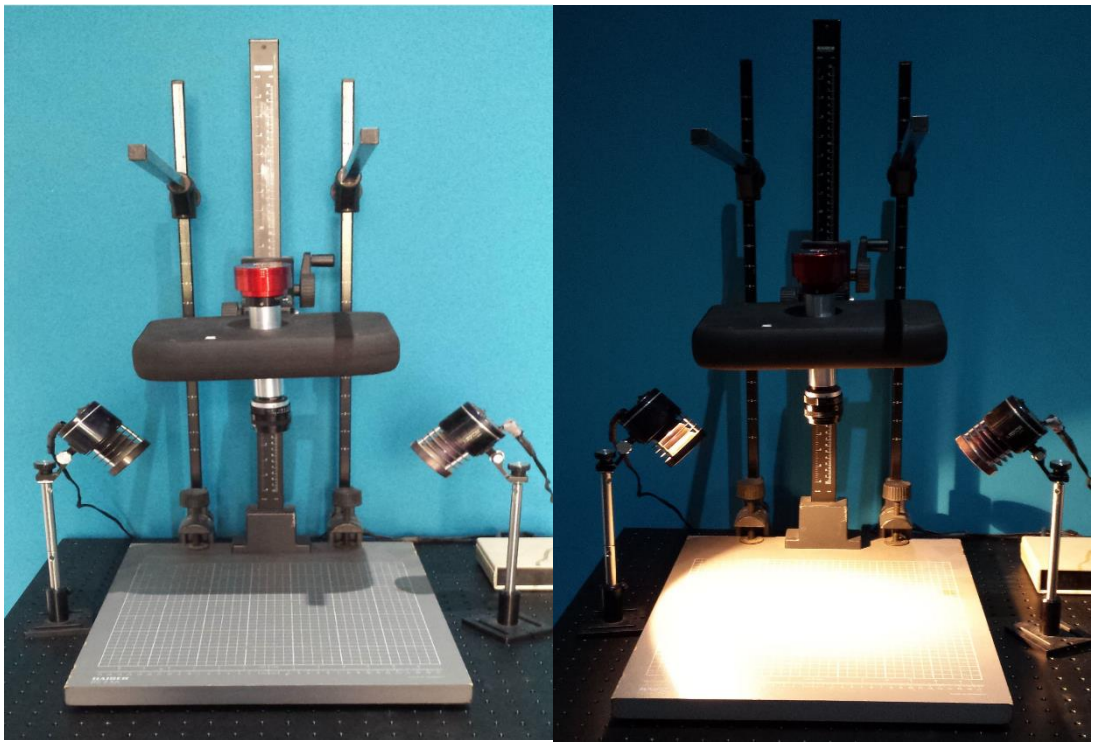

Figure 5. 21: Image Acquisition System Model

MUSES9-HS is a **staring** hyperspectral imager. The heart of this camera model is an **electro-optic filter module** (EOFM) that selects and tunes the imaging central wavelength. The EOFM is synchronized with the imaging sensor(s), so that several images are captured during **spectral scanning**. The acquired dataset (spectral cube) comprise the basis for calculating the spectra in every, pixel-size image location. Notably, in every tuning step, **live spectral images** are immediately available for **real time spectral inspection**.

Competing technologies, based on the spatial scanning of a point or a line spectrometer (push broom systems) cannot generate live spectral images, while, at the same time, the camera

and scanning package is bulky and heavy. As such, they are suitable mostly for table-top, indoor applications.

The **staring and portable design** of MUSES9-HS is clearly advantageous over traditional solutions, by providing live spectral image inspection and handheld operation. This expands the addressable range of applications and allows for examining precious samples in their natural location.

The MUSES9-HS software offers **high level of automation**, requiring no technical skills for system's operation. It also offers advanced tools for **spectral classification,** which generates and displays **spectral maps** depicting the **spectral topography** of the sample/scene. Importantly, when this is combined with **spectral libraries** and proper **machine learning models**, the system's analytical capabilities are greatly improved.

Basic Specifications:

- 4-6 Megapixels C-MOS @ 25 f/s (Plus InGaAs sensor for model-**HS1700**) in the 370-1100nm spectral range (370-1700nm for model-**HS1700**)
- 5-20 nm FWHM and 2-5nm tuning step
- >150 spectral images 4-6 millions of spectra
- 5-15 s scanning time
- Spectral and color imaging
- USB 3 interface
- Integrated software for camera control image handling, achieving and processing and spectral mapping
- accepts all kinds of lenses and microscopes
- low power-battery operation is supported

5.3.2 Results

We collect 21 images at range of 400nm to 1000nm per 30nm from the hand area between wrist and elbow. The diagram below shows the resulting mean RMSE value at each image band which extracted from RMSE values in four directions as we explained previously. We suppose that higher mean RMSE value shows more details about skin texture condition.

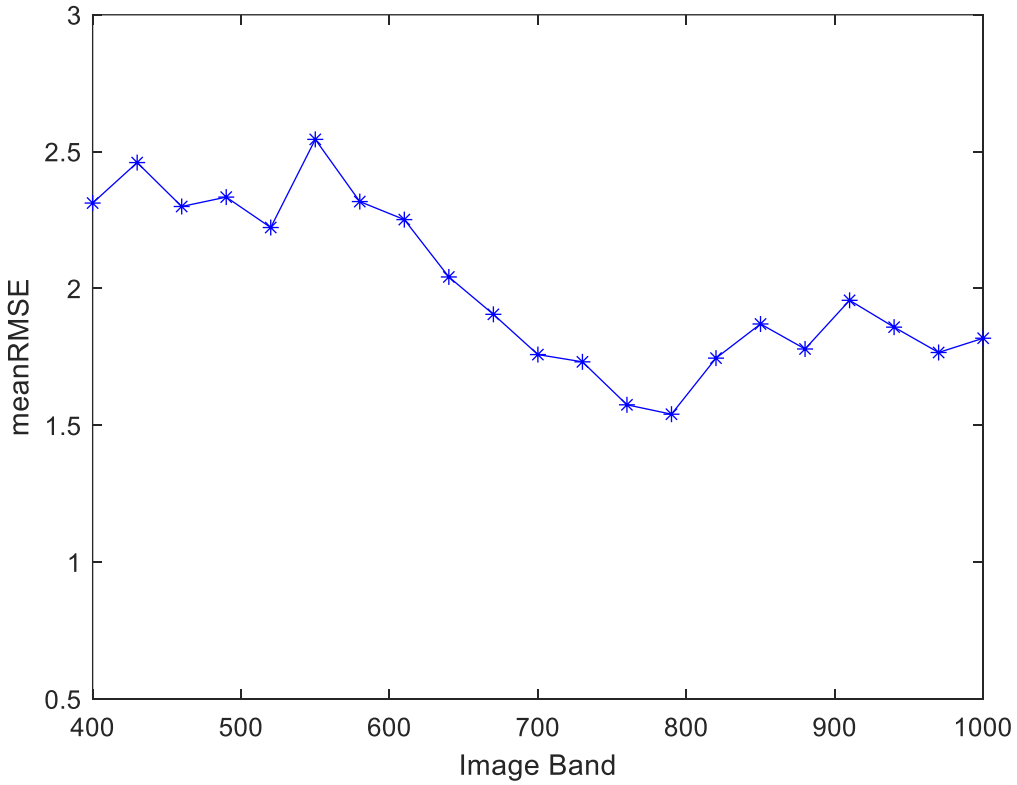

Figure 5. 22: The resulting RMSE value of 21 images which collected at each wavelength in the range of 400nm-1000nm.

Looking at Figure 5.22 and the corresponding Table 5.4 below we observe that the maximum peak of mean RMSE value is at 550nm.
Image at channel of 550nm shows also a high mean RMSE value which means more details about skin condition. From the results obtained using the Qcell Snapshot Hyperspectral Dermoscope, the maximum RMSE values and the corresponding mean RMSE value show at image of 540nm. The results obtained by the HSI system confirm that the images at 540-550nm are suitable to measure and quantify the condition of the skin texture. This will help in the objective diagnosis by the dermatologists and in the selection of the appropriate treatment depending on the degree of skin texture damage.

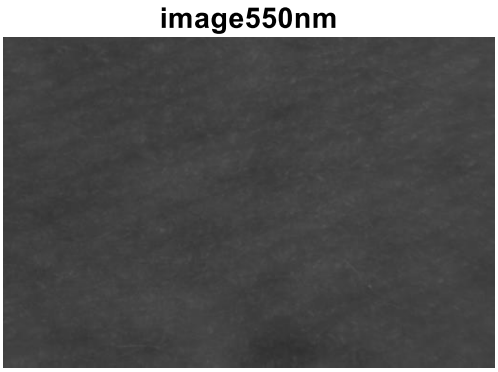

Figure 5. 23: Image at the maximum peak of mean RMSE value

Image band(nm)	RMSE 0^o	RMSE 45^o	RMSE 90^o	RMSE 135^o	Mean RMSE value
400	2,21	2,55	2,08	2,42	2.34
430	2,32	2,59	2,18	2,74	2.46
460	2,23	2,16	2,55	2,26	2.29
490	2,15	2,54	2,36	2,27	2.33
520	1,91	2,35	2,17	2,45	2.22
550	2,45	2,63	2,46	2,61	**2.54**
580	2,39	2,47	2,07	2,32	2.31
610	2,31	2,25	2,27	2,17	2.25
640	1,91	2,19	2,00	2,06	2.04
670	1,79	2,09	1,93	1,82	1.90
700	1,75	1,71	1,87	1,69	1.75
730	1,71	1,73	1,78	1,70	1.73
760	1,36	1,54	1,78	1,61	1.57
790	1,55	1,52	1,52	1,56	1.54
820	1.85	1.64	1.68	1.83	1.74
850	1,86	1,81	2,03	1,77	1.87
880	1,92	1,82	1,75	1,62	1.77
910	2,03	2,06	1,65	2,08	1.95
940	1,80	1,88	1,73	2,01	1.85
970	1,72	1,78	1,69	1,86	1.76
1000	1,87	1,91	1,83	1,66	1.81

Table 5. 4: RMSE values in all directions and the corresponding mean RMSE for each image band

Part 6: Conclusion and Future Work

The major benefit of hyper-spectral imaging is that an entire spectrum of information is acquired at every pixel of the object being examined. It is a non-destructive and non-invasive method, and hence could be used for on-line quality inspection and monitoring. The main advantage of hyper-spectral imaging is that it is possible to visualize the various biochemical components present in a sample based on spectral signature in a region of specific chemical composition where spectral properties may be similar.

Although, Hyperspectral Imaging has some disadvantages. The primary disadvantages are cost and complexity. It requires fast computers, sensitive detectors, and large data storage capacities in order to analyze hyperspectral data. It also necessary to contain Significant data storage capacity, since hyperspectral cubes are large, multidimensional datasets, potentially exceeding hundreds of megabytes. All of these factors greatly increase the cost of acquiring and processing hyperspectral data.

Hence, availability of a new diagnostic tool in aesthetic medicine, such as a dermoscope, have a high potential in the objective diagnosis and assessment of the skin texture and aging process related to its. The benefits of the dermoscope devices are that they are hand held and cheaper devices which have the ability to consist of spectral cameras which outputs specific spectrums and in connection with a digital computer can capture not only the appearance of human skin texture but also measure it in less time, using real-time applications in combination with effective image processing algorithm.

In this thesis, it has been proven, that RMSE is more efficient method in comparison with the most widely used algorithms and methods of skin texture aging quantification so far. The aim of current study is not only to quantify skin condition but also to introduce a hyperspectral imaging device and the method for monitoring age-related human skin topographical and in vivo changes. The results show that spectral images at 540 & 550nm can be used to analyze the condition of skin texture and provide better and more objective results in the evaluation of skin by dermatologists. By extracting a texture quantification index, such as RMSE value as demonstrated in this study, even an inexperienced specialist can assess skin texture damage and provide appropriate treatment.

Not only does RMSE represent a useful tool for evaluating skin texture in respect to age but it could also be useful for investigating before/after comparisons of topically treated skin. In addition, many others skin areas of the human body which have different skin texture topography and pattern could be investigated for both women and men separately from all of ages, using our method in order to correlate the RMSE value with age. Moreover, a hair removal algorithm will be very useful for automatic hair removal on a skin texture image, which affected by them and creates false results at the value of quantification index (in our case at the RMSE value).

Finally, all the above can form the basis for the development of innovative screening medicine and self-management medicine. Thus, the development of new optical diagnostic methods has potential to find promising application in aesthetic medicine. By means of Root Mean Square Error (RMSE) value, it was possible to quantify skin texture variations that correlated with the aging process.

References

[1] encyclopædia britannica: Spectroscopy definition
https://www.britannica.com/science/spectroscopy

[2] T. Vo-Dinh. Biomedical Photonics Handbook, Taylor & Francis, 2010.

[3] D. A. Boas, C. Pitris, and N. Ramanujam. Handbook of Biomedical Optics, chapter 7, pages 131-164. Taylor & Francis, 2011.

[4] Goetz AF, Vane G, Solomon JE, Rock BN. Imaging spectrometry for Earth remote sensing. Science. 1985; 228:1147-1153

[5] Zhang B, Huang W, Li J, Zhao C, Fan S, Wu J, Liu C. Principles, developments and applications of computer vision for external quality inspection of fruits and vegetables: A review. Food Research International. 2014; 62:326-343

[6] Arngren M, Schmidt MN, Larsen J. Unmixing of Hyperspectral images using Bayesian non-negative matrix factorization with volume prior. Journal of Signal Processing Systems. 2011;65:479-496

[7] Monteiro ST, Minekawa Y, Kosugi Y. Prediction of sweetness and amino acid content in soybean crops from hyperspectral imagery. Isprs Journal of Photogrammetry & Remote Sensing. 2007; 62:2-12

[8] Smail VW, Fritz AK, Wetzel DL. Chemical imaging of intact seeds with NIR focal plane array assists plant breeding. Vibrational Spectroscopy. 2006;42:215-221

[9] Uno Y, Prasher SO, Lacroix R, Goel PK, Karimi Y, Viau A, Patel RM. Artificial neural networks to predict corn yield from compact airborne spectrographic imager data. Computers & Electronics in Agriculture. 2005; 47:149-161

[10] Chang CI. Hyperspectral Imaging: Techniques for Spectral Detection and Classification. Plenum Publishing Co; 2003

[11] V. V. Tuchin. \Handbook of Coherent-Domain Optical Methods: Biomedical Diagnostics, Environmental Monitoring, and Materials Science". Springer-Verlag GmbH, 2013.

[12] Quantitative evaluation methods of skin condition based on texture feature parameters. Hui Pang, Tianhua Chen *, Xiaoyi Wang, Zhineng Chang, Siqi Shao, Jing Zhao. Saudi J. Biol. Sci. 24(3), 514-518 (2007)

[13] Irregularity skin index (ISI): a tool to evaluate skin surface texture. Michele Setaro and Adele Sparavigna DermIng, Institute of Dermatological Research and Bioengineering, Milan, Italy, Skin Research and Technology 2001; 7: 159–163

[14] Measurement of skin texture through polarization imaging P.R. Bargo and N. Kollias. Journal Compilation 2010 British Association of Dermatologists British Journal of Dermatology 2010 162, pp724–731

[15] https://www.canfieldsci.com/imaging-systems/visia-complexion-analysis/

[16] https://www.quantificare.com/3d-photography-systems/lifeviz-micro/

[17] https://www.btbp.org/Clarity2D&3DResearchSystem.html

[18] http://miravex.com/antera-3d/